THE JOURNAL OF BIOLOGICAL CHEMISTRY VOL. 287, NO. 35, pp. 29479–29494, August 24, 2012

Selective Inhibition of CCR7$^-$ Effector Memory T Cell Activation by a Novel Peptide Targeting Kv1.3 Channel in a Rat Experimental Autoimmune Encephalomyelitis Model*

Received for publication, May 8, 2012, and in revised form, June 25, 2012 Published, JBC Papers in Press, July 3, 2012, DOI 10.1074/jbc.M112.379594

Zhi Li[‡1], **Wan-Hong Liu**[‡1], **Song Han**[‡], **Bi-Wen Peng**[‡], **Jun Yin**[‡], **Ying-Liang Wu**[§2], **Xiao-Hua He**[‡3], **and Wen-Xin Li**[§]

From the [‡]*Hubei Province Key Laboratory of Allergy and Immunology, School of Basic Medical Sciences, Wuhan University, Wuhan 430071 and the* [§]*State Key Laboratory of Virology, College of Life Sciences, Wuhan University, Wuhan 430072, China*

Background: The effect of ADWX-1 on EAE model is unknown.
Results: ADWX-1 selectively inhibits T_{EM} activation through regulating both Kv1.3 activity and expression.
Conclusion: ADWX-1 ameliorates EAE with a cell selectivity mechanism.
Significance: ADWX-1 is a novel potent candidate therapeutic drug for MS.

The voltage-gated Kv1.3 K^+ channel in effector memory T cells serves as a new therapeutic target for multiple sclerosis. In our previous studies, the novel peptide ADWX-1 was designed and synthesized as a specific Kv1.3 blocker. However, it is unclear if and how ADWX-1 alleviates experimental autoimmune encephalomyelitis, a model for multiple sclerosis. In this study, the administration of ADWX-1 significantly ameliorated the rat experimental autoimmune encephalomyelitis model by selectively inhibiting $CD4^+CCR7^-$ phenotype effector memory T cell activation. In contrast, the Kv1.3-specific peptide had little effect on $CD4^+CCR7^+$ cells, thereby limiting side effects. Furthermore, we determined that ADWX-1 is involved in the regulation of NF-κB signaling through upstream protein kinase C-θ (PKCθ) in the IL-2 pathway of $CD4^+CCR7^-$ cells. The elevated expression of Kv1.3 mRNA and protein in activated $CD4^+CCR7^-$ cells was reduced by ADWX-1 engagement; however, an apparent alteration in $CD4^+CCR7^+$ cells was not observed. Moreover, the selective regulation of the Kv1.3 channel gene expression pattern by ADWX-1 provided a further and sustained inhibition of the $CD4^+CCR7^-$ phenotype, which depends on the activity of Kv1.3 to modulate its activation signal. In addition, ADWX-1 mediated the activation of differentiated Th17 cells through the $CCR7^-$ phenotype. The efficacy of ADWX-1 is supported by multiple functions, which are based on a $Kv1.3^{high}$ $CD4^+CCR7^-$ T cell selectivity through two different pathways, including the classic channel activity-associated IL-2 pathway and the new Kv1.3 channel gene expression pathway.

Multiple sclerosis (MS)[4] is a typical autoimmune disease in which inflammatory cells from the peripheral blood invade the central nervous system (CNS) and actively attack axons, myelin sheaths, and oligodendrocytes (1, 2). The neurological disability caused by the demyelination of the axons afflicts millions of young people (3). However, the current MS therapies are expensive, are only partially effective, and are associated with side effects as well as potential toxicity; therefore, there is a need for clinical treatments that can efficiently prevent neuronal injury by attenuating the acute autoimmune exacerbations that occur in the early stages of MS.

Although the pathogenesis of MS is complicated and remains uncertain, among the multiple immune cells that participate in the development of the disease, T lymphocytes play a dominant role. In MS, the infiltrated T lymphocytes that disrupt the blood-brain barrier recognize the specific myelin antigens in the CNS where cells are restimulated. Therapies targeting the recruitment of reactive T cells in the CNS exhibit further immune modulatory effects to prevent inflammatory cytokine secretion and the neurologic deficits caused by demyelination (4, 5).

Recently, the voltage-gated potassium channel Kv1.3 was proposed as a promising new therapeutic target for MS because the numbers of Kv1.3 on autoimmune disease-related $CCR7^-$ effector memory T cells (T_{EM}) increase significantly after activation by myelin antigens (6–8). The naive $CCR7^+$ T cells differentiate into auto-reactive $CCR7^-$ T cells by repeated autoantigen stimulation. These cells migrate into inflamed tissues and exhibit immediate effector functions, such as inflammatory cytokine secretion (5). Therefore, it is possible that the selective suppression of T_{EM} cells using specific Kv1.3 blockers could efficiently suppress these immune responses and alleviate MS. The toxin peptides (*e.g.* ShK-F6CA (9), OSK1 (10), margatoxin (11), etc.) derived from naturally venomous animals exhibit

* This work was supported by the National Basic Research Program of China Grant 2010CB529803, the National Natural Sciences Foundation of China Grants 81171127, 31000344, and 81171577, the National Science and Technology Major Projects of New Drugs Grants 2012ZX09103301-028, the Natural Science Foundation of Hubei Province of China Grant 2010CDA045, Fundamental Research Funds for the Central Universities, and National High Technology Research and Development Program of China (2012AA020304).

[1] Both authors contributed equally to this work.
[2] To whom correspondence may be addressed: State Key Laboratory of Virology, College of Life Sciences, Wuhan University, Wuhan 430072, China. Tel.: 86-27-68752831; Fax: 86-27-68752146; E-mail: ylwu@whu.edu.cn.
[3] To whom correspondence may be addressed: School of Basic Medical Sciences, Wuhan University, Donghu Rd, No. 185, Wuchang, Wuhan 430071, China. Tel.: 86-27-68759991; E-mail: hexiaohua@whu.edu.cn.

[4] The abbreviations used are: MS, multiple sclerosis; EAE, experimental autoimmune encephalomyelitis; T_{EM}, effector memory T cells; PBMC, peripheral blood mononuclear cells; CFSE, carboxyfluorescein diacetate succinimidyl ester; MBP, myelin basic protein; MFI, mean fluorescent intensity; CDZ, calmidazolium; PE, phycoerythrin; FCM, flow cytometry; CsA, cyclosporin A.

greater potency (with picomolar affinity) and selectivity on Kv1.3 blockade than small chemical molecules (*e.g.* Psora-4 (12), correolide (13), etc.) designed to block Kv1.3 (at nanomolar concentrations) (14). Currently, the newly designed Kv1.3 blocker peptides (*e.g.* Moka-1 (15), ShK (L5) (5), etc.) were synthesized to target the Kv1.3 channel as a new therapy for MS. However, novel peptides remain required for sufficient specificity to distinguish between Kv1.3 and other related Kv1.*x* channels (16, 17). Moreover, although Kv1.3 blocker peptides, such as ShK (a 35-AA polypeptide isolated from the sea anemone *Stichodactyla helianthus*), efficiently attenuate the severity of experimental autoimmune encephalomyelitis (EAE), a model for MS (18, 19), the mechanisms underlying the peptide-mediated inhibition of activation and proliferation of primary T_{EM} cells derived from the EAE model are poorly understood.

In a previous study, we developed the novel Kv1.3 blocker peptide ADWX-1 as a representative drug with a high affinity, high potency, and selectivity toward the Kv1.3 channel (20, 21). This peptide is based on the natural scorpion toxin BmKTX in which three important residues were mutated in a structure-modification strategy to enhance the Kv1.3 channel selectivity (20). ADWX-1 blocked Kv1.3 currents with an IC_{50} of 1.89 pM and displayed specificity for Kv1.3 over Kv1.1 and Kv1.2 (20). However, to develop new drug treatments for MS in a clinical setting, further functional studies of ADWX-1 in the animal model of MS are required. In this study, we first examined whether ADWX-1, the Kv1.3-targeting peptide, ameliorated the EAE model. Next, we elucidated the effects of ADWX-1 on T cell activation in the EAE model focusing on the selective effect on T_{EM} cells and the T_{EM} cell activation pathways involved.

EXPERIMENTAL PROCEDURES

Peptide Expression and Purification—ADWX-1 peptide was obtained as described previously (20). The molecular mass of the purified ADWX-1 peptide was obtained by MALDI-TOF-MS (Voyager-DESTR, Applied Biosystems). Peptide purity was >95%.

Animals and Cell Culture—Female inbred 8–10-week-old Sprague-Dawley (SD) rats were purchased from the ABSL-III laboratory at Wuhan University and were housed under specific pathogen-free conditions. All animal work was performed in accordance with protocols and guidelines approved by the Institutional Animal Care and Use Committee.

The Jurkat T cells were purchased from the China Center for Type Culture Collection. Ficoll gradients were used to isolate splenocytes and peripheral blood mononuclear cells (PBMCs) from rats. The $CD4^+$ T cells from PBMCs were purified using MACS (Miltenyi Biotech). The separated cells were sorted into $CCR7^-$ and $CCR7^+$ subsets using FACS. The primary T cells or total PBMCs were seeded at 10^5/well with 10^5 irradiated autologous PBMCs (3,000 rads) in a volume of 200 μl/well in round-bottom 96-well plates. The cells were cultured in 1640 RPMI medium supplemented with 2 mM glutamine, 100 units/ml penicillin, 100 μg/ml streptomycin, and 1% homologous rat serum at 37 °C. The T cells derived from the EAE rats were incubated with the Kv1.3 blocker ADWX-1 for 60 min and were stimulated with the myelin-specific antigen myelin basic protein (MBP) (5 μg/ml) for 48–72 h. The T cells derived from control rats or the peripheral blood of healthy donors were stimulated with soluble anti-CD3 antibody (Ab) (1 μg/ml) (eBioscience) or PHA (Sigma).

Rat EAE Induction and Drug Administration—The EAE model was induced using homologous homogenates extracted from the brain and spinal cord of SD rats. Homogenates containing 25 μg of brainstem and spinal cord extracts and 50 μl of PBS were emulsified in 50 μl of complete Freund's adjuvant (Sigma) supplemented with 0.4 mg of *Mycobacterium tuberculosis* (H37RA). The footpad of each rat was immunized by the subcutaneous injection of this emulsion at a dose of 150 μl/200 g and with an auxiliary injection of 0.2 ml of pertussis toxin. Control rats received PBS plus complete Freund's adjuvant, and the second immunization was administered 7 days after the first injection. The rats were weighed and observed daily. In the prevention trial, the rats were subcutaneously injected once daily with 100 μg/kg ADWX-1 in 1 ml of PBS from days 0 to 4. In the treatment trial, ADWX-1 was administered after the onset of disease for 3 days of continued therapy. The vehicle group received PBS. The clinical scores were recorded daily as follows (19): 0 = no clinical signs; 0.5 = distal limp tail; 1 = limp tail; 2 = mild paraparesis or ataxia; 3 = moderate paraparesis; 4 = complete hind leg paralysis or severe ataxia; 5 = 4+ incontinence; 5.5 = tetraplegia; 6 = death. Special care was required for animals with severe EAE (score of 3 or more).

Ca^{2+} Measurement—The $[Ca^{2+}]_i$ in lymphocytes was calculated as described previously (18), and T cells were attached to an L-lysine-coated glass dish and loaded with 1 μM Fura-2 AM (Dojindo, Japan) for 60 min, and then cells were washed and incubated with 1 or 10 nM ADWX-1 or 0.1% bovine serum albumin (BSA, Sigma) for 50 min. After antigen stimulation with MBP or anti-CD3 Ab in Ca^{2+}-rich medium, the intracellular calcium concentrations were determined by fluorescence intensity. The fluorescence excitation wavelength was set at 480 nm, and emission wavelength was set at 530 nm.

Cell Proliferation—10^6 PBMCs were seeded in round-bottom 96-well plates (Corning-Costar) and were incubated with 50 or 250 μg/ml homogenate antigen in 200 μl of culture medium supplemented with 1% homologous rat serum. ADWX-1 at various concentrations (0.1, 1, and 10 nM) was added 60 min before antigen stimulation. The cells were cultured for 4 days and were pulsed with [^{3}H]thymidine) (1 μCi per well) 16 h before harvesting. The proliferative response was assessed using a β-scintillation counter (Beckman) to measure the [^{3}H]thymidine incorporation (counts/min value) as follows: background counts in unstimulated (resting) cells were below 600 cpm, and counts in only antigen-activated (maximal) cells were 60,000–80,000 cpm.

In vitro generated $CD4^+CCR7^-$ T_{EM} cells were suspended in PBS at a concentration of 10^7 cells/ml and were incubated at 37 °C for 10 min with carboxyfluorescein diacetate succinimidyl ester (CFSE, Molecular Probes) at a final concentration of 1 μM. The cells were washed, resuspended in medium, and stimulated with antigen. The fluorescence intensity of the CFSE was measured by flow cytometry (FCM) after 4 days (22).

For the signal transduction study, $CD4^+CCR7^-$ T cells derived from the PBMCs of EAE rats were incubated for 60 min

with 1 μM cyclosporin A (CsA, Sigma) or 30 μM rottlerin (Sigma) or 25 μM pyrrolidine dithiocarbamate (Sigma) and were stimulated with MBP for 4 days. ADWX-1, 1 or 10 nM, was added 60 min before antigen stimulation. The proliferative response was determined by 3-(4,5-dimethylthiazol-2-yl)-2,5-diphenyltetrazolium bromide assay using a Cell Counting Kit-8 (CCK-8, Dojindo, Japan).

Flow Cytometry—The PBMCs from each group in the *in vivo* study were directly double-stained directly using PE-Cy5-labeled anti-rat CD4 mAb (Pharmingen) and rabbit anti-CCR7 antibody (Abcam) followed by a secondary PE-conjugated goat anti-rabbit IgG. The PBMCs cultured *in vitro* were collected after 4 days and were double-stained using PE-Cy5-CD4 and PE-CCR7. The stained cells were analyzed by FCM (Beckman Coulter, Epics Altra II). To determine the Kv1.3 protein expression, the PBMCs cultured *in vitro* were harvested after 48 h and were triple-stained with PE-Cy5-CD4, PE-CCR7, as well as FITC-conjugated anti-Kv1.3 antibody (Sigma, P4247). The Kv1.3 mean fluorescence intensity (MFI) values were measured using FCM; the PBMCs isolated *in vivo* were directly stained directly with FITC-Kv1.3 antibody for the FCM assay.

Quantitative RT-PCR—Freshly purified $CD4^+CCR7^-$ and $CD4^+CCR7^+$ T cells from PBMCs were activated *in vitro* for 48 h, and the cells were resorted into $CD4^+CCR7^-$ and $CD4^+CCR7^+$ populations for quantitative RT-PCR analysis. The RNA was isolated from the cells using TRIzol reagent (Invitrogen), and reversed transcription was performed using the First Strand cDNA synthesis kit (Fermentas), in accordance with the manufacturer's instructions. Total PBMC samples triple-stained for the Kv1.3 MFI test were also sorted into $CD4^+CCR7^-$ and $CD4^+CCR7^+$ populations for quantitative RT-PCR analysis. The expressions of the gene encoding *KCNA3* (Kv1.3 channels) were quantified using the SYBR Green PCR master mix kit (Toyobo). The following primer pairs were selected for the amplification of *KCNA3* gene: forward, 5′-AGTATATGGTGATCGAAGAGG-3′, and reverse, 5′-AGTGAATATCTTCTTGATGTT-3′. The reactions were performed on an ABI 7500 platform under the following conditions: 95 °C for 5 s, 55 °C for 8 s, and 72 °C for 9 s, preceded by 10 min at 95 °C and followed by 10 min at 95 °C. Melting curves were performed to verify the specificity of the product, and primers for *GAPDH* were included as an internal reference. The relative gene expression was determined as the ratio of *KCNA3* to *GAPDH* gene expression for each sample.

ELISA—IL-2 levels from the supernatants of the cell cultures were measured using ELISA. Supernatants of cell cultures were collected 16 h after antigen stimulation. Cytokine levels were measured using rat and human IL-2 and IFN-γ Quantikine kits (R&D Systems) according to the manufacturer's instructions. The IL-2, IFN-γ, and TNF-α cytokine production in serum from each group of animal experiments (on day 15) was also assessed by rat Quantikine kits (R&D Systems). Homogenates of rat brain and spinal cord were used to assay the IL-2 levels in tissues by rat IL-2 Quantikine kit (R&D Systems).

T Cell Differentiation—Naive $CD4^+$ T cells from rats, sorted using FACS, were stimulated for 4–5 days with anti-CD3/CD28 beads (Miltenyi Biotec) plus the following recombinant cytokines: TGF-β (5 ng/ml, PeproTech) and IL-6 (10 ng/ml, PeproTech) for polarization of the T cells into the Th17 subset. The cells were incubated with 1 or 10 nM ADWX-1 for 60 min before differentiation. The cells were harvested and double-stained with PE-Cy5-labeled anti-rat CD4 mAb (Pharmingen) and PE-labeled anti-rat IL-17A mAb (eBioscience). The differentiated cells were double-stained with PE-labeled anti-rat IL-17A mAb and rabbit anti-CCR7 antibody (Abcam) followed by a secondary FITC-conjugated goat anti-rabbit IgG. The differentiated cells were restimulated using anti-CD3 Ab alone, and ADWX-1 was added; the expression of $CD4^+IL\text{-}17^+$ Th17 cells was determined after 3 days. The supernatants from primary differentiated cultures were collected on day 4, and the restimulated cultures were collected after incubation overnight. IL-17 production was assessed using ELISA kit (eBioscience). $CD4^+$ T cells were activated using anti-CD3 Ab, and ADWX-1 was added; the expression of $CD4^+Foxp3^+$ Treg cells was determined after 3 days following the intracellular staining of Foxp3 (eBioscience). For the *in vivo* study, the PBMCs from each group were isolated and stained directly for the FCM assay of the percentage of $CD4^+IL\text{-}17^+$ and $CD4^+Foxp3^+$ cells without incubation. On day 15, IL-17 and TGF-β cytokines in the serum or the homogenates were measured using ELISA.

Western Blotting—In signaling transduction study, $CD4^+CCR7^-$ T cells from EAE rats were incubated with the indicated compound (rottlerin, pyrrolidine dithiocarbamate) as well as 1 or 10 nM ADWX-1 for 1 h, and then stimulated *in vitro* by myelin antigen MBP for 4 h. Cells were lysed by RIPA plus 0.1% pepstatin, aprotinin, leupeptin, and 0.1% PMSF for Western blotting analysis. The concentration of proteins was determined by Bradford assay before the lysate was boiled with loading buffer. Proteins were separated on a 10% SDS-polyacrylamide gel and then were transferred to PVDF membranes under 100 V for 80 min (Immobilon-P, Millipore). Membranes were blocked in 5% milk TBST for 1 h. NF-κB activity was determined by phospho-NF-κB p65 (Ser-536) (93H1) rabbit mAb (Cell Signaling) followed by a second antibody of HRP-conjugated goat anti-mouse IgG (Santa Cruz Biotechnology). The membranes were developed using an ECL kit (Pierce) according to the manufacturer's instructions. For the Kv1.3 membrane protein expression study, mouse monoclonal (S23-27) antibody to KCNA3 (Abcam) was used for membrane blot, and monoclonal anti-β-actin antibody (Sigma) was used as control.

Histology—For H&E staining and Luxol fast blue staining, rats were anesthetized with 10% chloraldurate and then perfused transcardially by 0.9% NaCl and pre-fixed with 4% paraformaldehyde in 0.1 M PBS. The lumbar region of the spinal cord and brainstem were collected and fixed in paraformaldehyde solution. The tissues were embedded in paraffin and cut into transverse sections (5 μm) that were stained by hematoxylin and eosin (H&E) to evaluate inflammatory cell distribution and by Luxol fast blue to evaluate demyelination. The number of perivascular inflammatory infiltrates and the degree of demyelination per section were calculated by two blinded investigators as histological scores (23, 24) as follows: grade 1 refers to less than 25% infiltration or demyelination; grade 2 denotes over 25% infiltration or demyelination, and grade 3 denotes widespread infiltration or demyelination. For T_{EM}

analysis, tissues were fixed in 3% glutaraldehyde and 1% osmium tetroxide and embedded in Epon 812 to make ultrathin sections that were counterstained by uranyl acetate and lead citrate and then examined in a transmission electron microscope (Hitachi) at 80 kV.

Statistical Analysis— The differences between groups were evaluated using a Student's *t* test or a one-way analysis of variance followed by a Dunnett's test for multiple comparisons. The one-way analysis of variance was used to compare the clinical score between two groups at every time point and was followed by a Mann-Whitney *U* test to determine the differences between the two curves in the EAE study. *p* values less than 0.05 were considered statistically significant. The data were analyzed using the GraphPad Prism software.

RESULTS

ADWX-1 Has a Therapeutic Effect on Rat EAE Model in Vivo and in Vitro—Previously, we designed and synthesized a novel ADWX-1 peptide as a specific Kv1.3 blocker and found that this peptide displayed high potency and selectivity toward Kv1.3 when compared with the related Kv1.1 and Kv1.2 channels (20). To evaluate whether the Kv1.3-specific peptide ADWX-1 is a viable therapeutic agent for the treatment of MS, a rat EAE model was employed to simulate the human MS disease. The rat EAE model is more appropriate than the mouse EAE model, because the Kv1.3 expression pattern in mice differs from humans and is not suitable for evaluating the effects of Kv1.3 blockers (25).

Stable symptoms of acute EAE were induced by immunizing Sprague-Dawley rats. These rats developed an ascending paralysis from day 7 to 14 post-immunization, and the clinical signs peaked at days 11–14 (Fig. 1*A*). For the prevention trial and the treatment trial, the EAE rats received a subcutaneous injection of 100 μg/kg/day ADWX-1. In the prevention trial, the ADWX-1-pretreated rats exhibited significantly reduced neurological scores compared with vehicle-treated rats on days 10 ($p < 0.01$), 11 ($p < 0.001$), 12 ($p < 0.001$), 13 ($p < 0.001$), and 14 ($p < 0.01$, Fig. 1*A*). In the treatment trial, the ADWX-1-treated rats also showed greatly reduced neurological scores compared with the vehicle-treated rats on days 10 ($p < 0.05$), 11 ($p < 0.001$), 12 ($p < 0.0001$), 13 ($p < 0.01$), and 14 ($p < 0.001$, Fig. 1*A*). Interestingly, the clinical scores of the prevention group were also significantly lower than the vehicle group on days 10–14, exhibiting a delayed onset and delayed peak day for the disease, suggesting that the peptide may modulate T cell autoactivation peripherally. In addition to the neurological score, significant reductions in inflammatory infiltrates ($p < 0.001$) and demyelination ($p < 0.05$) in the affected spinal cord, as shown by the histological score, were observed in the ADWX-1-treated EAE rats compared with the vehicle-treated rats (Fig. 1*B*). The transmission electron microscopy analysis revealed that the ultrastructure of the tissue in ADWX-1-treated rats contained less demyelinated axons compared with the vehicle-treated rats (Fig. 1*C*).

Considering the importance of Th1-type cytokines, such as IL-2, IFN-γ, and TNF-α during the development of autoimmune disease, various inflammatory cytokines in the serum were analyzed. In the prevention group and the treatment group, IL-2 and IFN-γ productions observed after ADWX-1 engagement were less than that observed in the vehicle-treated rats but higher than that in the control rats (Fig. 1*D*). Furthermore, the down-regulation of IL-2 in the CNS of the ADWX-1-treated rats further supports that ADWX-1 attenuates cellular infiltration in pathological tissues, including the brainstem and the spinal cord (Fig. 1*E*).

To confirm the decrease in inflammatory cytokines in the ADWX-1-treated EAE rats, we investigated whether ADWX-1 suppresses T cell activation and proliferation in isolated PBMCs *in vitro*. Using ELISA, we observed that inflammatory IL-2 secretion in MBP-stimulated PBMCs from EAE rats treated with ADWX-1 (0.01, 0.1, 1, and 10 nM) *in vitro* was markedly decreased compared with non-ADWX-1-treated cells in a dose-dependent manner (Fig. 1*F*). However, the T cell response of PHA-stimulated PBMCs from the control rats treated with ADWX-1 (0.01, 0.1, 1, and 10 nM) *in vitro* was not altered compared with non-ADWX-1-treated cells (Fig. 1*F*). These results suggest that the suppression of myelin-specific T cell activation *in vitro* supports the modulation of inflammatory cytokines by ADWX-1 *in vivo*. Furthermore, ADWX-1 inhibited the EAE rat T cell proliferation triggered by high and low concentrations of myelin antigen in a dose-dependent manner (Fig. 1*G*).

These *in vivo* and *in vitro* data demonstrate that ADWX-1 significantly alleviates EAE. Considering that both the efficacy and safety are crucial issues for long term drug therapies and that the Kv1.3 blocker peptides are toxins derived from naturally venomous animals, we performed 2-week acute toxicity studies using 50- or 100-fold doses of ADWX-1 (5 or 10 mg/kg). These doses failed to induce pathological changes in the behavior or tissues of the rats (data not shown).

ADWX-1 Preferentially Inhibits T Cell Activation and Proliferation in $CD4^+CCR7^-$ T Cells—The amelioration of the EAE model by the ADWX-1 peptide prompted us to delineate the possible mechanisms underlying the therapeutic effects of this peptide. We addressed the molecular mechanisms starting with the critical finding that $CD4^+CCR7^-$ T_{EM} cells in the EAE model were specifically inhibited by ADWX-1 engagement. A 2-fold up-regulation of $CD4^+CCR7^-$ T_{EM} cells was observed in the EAE model as compared with the control animals (Fig. 2*A*), possibly because of the *in vivo* proliferation of the myelin antigen-specific T cells in this population. This hypothesis is consistent with the observation that patients carrying autoimmune diseases generate a high number of effector memory T cells with high expression of Kv1.3 (7, 25). However, the injection of 100 μg/kg/day of ADWX-1 decreased the number of $CD4^+CCR7^-$ T_{EM} cells by ~12% in the EAE model in both the prevention and treatment trials (Fig. 2*A*), indicating that ADWX-1 ameliorates the disease through the physiological modulation of $CCR7^-$ T_{EM} proliferation.

To elucidate the mechanism underlying the *in vivo* suppression of the $CCR7^-$ phenotype by the Kv1.3 blocker peptide ADWX-1, we investigated the effects of ADWX-1 on the *in vitro* immune responses of primary $CD4^+CCR7^+$ and $CD4^+CCR7^-$ T cell subsets purified from PBMCs.

A substantial amount of inflammatory IL-2, a marker of $CD4^+$ T cell activation, was produced in cultured MBP-stimu-

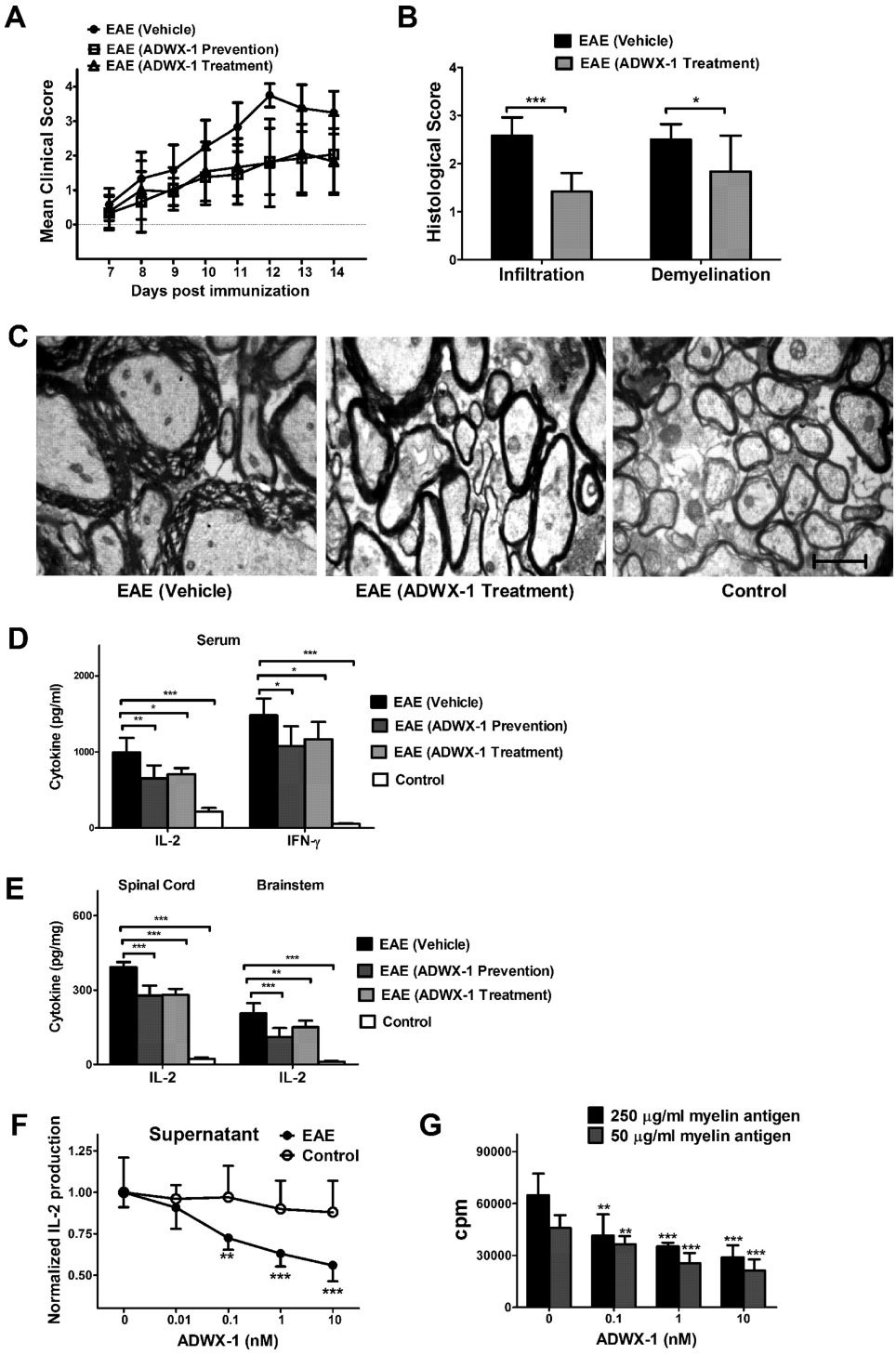

FIGURE 1. **Therapeutic effect of ADWX-1 on a rat acute EAE model.** *A,* prevention and treatment trial. Rats were immunized with myelin antigens on day 0; the prevention group (from day 0 to day 4) and treatment group (for 3 days after the onset of clinical signs) were subcutaneously injected with ADWX-1 at a dose of 100 μg/kg, and the vehicle group was injected with PBS ($n = 12$). The clinical score was recorded daily. *B,* statistical data for H&E staining and Luxol fast blue staining ($n = 6$) shown as the histological score depicting the inflammatory infiltration and demyelination in the spinal cord of EAE rats treated with ADWX-1 or PBS. *C,* representative photographs from transmission electron microscopy demonstrating demyelination and axonal loss in the spinal cord of the vehicle group, treatment group, and control group. *Scale bar,* 1,600 nm. *D,* Th1 type IL-2 and IFN-γ production in serum from each group ($n = 6$) was determined by ELISA. *E,* IL-2 production in CNS tissues from each group ($n = 6$) was determined by ELISA. **, $p < 0.01$; ***, $p < 0.001$ *versus* EAE (vehicle). *F,* cell activation *in vitro*. PBMCs from EAE (*black*) and control (*white*) rats were treated with various concentrations of ADWX-1 (0, 0.01, 0.1, 1, and 10 nM) for 1 h before activation with MBP or PHA for 16 h. IL-2 levels in the supernatants were assessed by ELISA. *G,* cell proliferation *in vitro*. PBMCs from EAE rats were treated with various concentrations of ADWX-1 (0, 0.1, 1, and 10 nM) and were activated for 96 h with high concentration (250 μg/ml, *black*) or low concentration (50 μg/ml, *gray*) of myelin antigen. **, $p < 0.01$; ***, $p < 0.001$ *versus* 0 nM ADWX-1. The data represent the mean ± S.D. from two independent experiments performed in triplicate.

lated $CD4^+CCR7^-$ T cells from EAE rats compared with resting cells from the same population ($p < 0.001$), whereas no IL-2 was produced by the $CD4^+CCR7^+$ subset ($p > 0.05$, Fig. 2*B*). However, the secretion of IL-2 upon activation *in vitro* was suppressed significantly (~50%) by the addition of 1 or 10 nM ADWX-1 in $CD4^+CCR7^-$ but not in $CD4^+CCR7^+$ T cells (Fig.

2*B*), suggesting that Kv1.3-related signaling pathways might be involved in the activation of the $CCR7^-$ subset. Similar effects of ADWX-1 were observed in the cells from control rats stimulated with anti-CD3 Ab (Fig. 2*C*). Similar results in IL-2 production were observed in the splenocytes of rats and in the human T cell line Jurkat T cells (data not shown). To determine whether ADWX-1 is specific to human $CD4^+CCR7^-$ T cells at a clinical level, we stimulated purified $CD4^+CCR7^-$ and

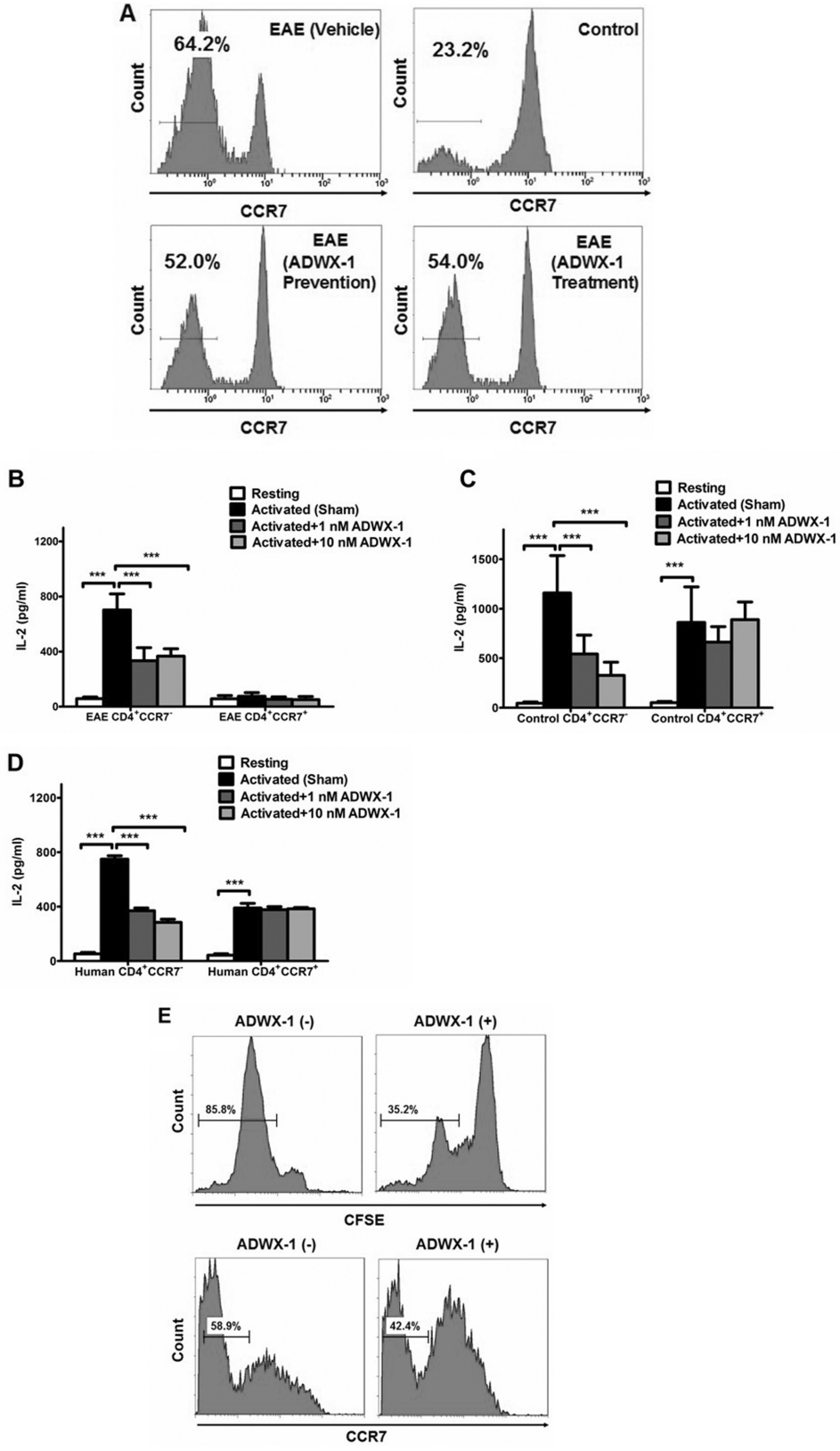

$CD4^+CCR7^+$ T cells from healthy individuals in the presence of ADWX-1. Similar to the rat cells, the ADWX-1 peptide affected the activation of the human $CCR7^-$ subset but not the $CCR7^+$ subset within the same $CD4^+$ population (Fig. 2*D*). In addition to IL-2, an analogous change in IFN-γ production was also observed (data not shown). These results suggest that ADWX-1 plays a selective role in the inhibition of $CD4^+CCR7^-$ T_{EM} activation in both rats and humans.

It is known that proliferation follows activation. We determined that ADWX-1 selectively inhibited the MBP-triggered proliferation of CFSE-labeled $CD4^+CCR7^-$ T cells from EAE rats (Fig. 2*E*), and the number of $CCR7^-$ cells in the CD4-gated cell population treated with ADWX-1 dropped after activation (Fig. 2*E*). These results further confirmed that ADWX-1 is more specific for $CD4^+CCR7^-$ T cells.

ADWX-1 Inhibits $CD4^+CCR7^-$ T Cell Activation through a Kv1.3-mediated IL-2 Activation Pathway—To further elucidate the molecular mechanism underlying the observed selective inhibition of $CD4^+CCR7^-$ T_{EM} cell activation by ADWX-1, we investigated the signaling activity of the IL-2 pathway, which is critical for the activation of T_{EM} cells. Previously, we determined that ADWX-1 targets the artificially expressed Kv1.3 channels in transfected cells and blocks the channel currents (20). Moreover, the voltage-gated Kv1.3 channels open for potassium efflux after antigen-induced depolarization, which promotes calcium influx through the calcium release-activated calcium channel (26, 27). To determine the effect of ADWX-1 on the initial calcium signaling for downstream IL-2 activation in antigen presentation, $[Ca^{2+}]_i$ was measured in accordance with methods described previously (18). It was observed that $CD4^+$ T cells from the EAE and control rats exhibited increased $[Ca^{2+}]_i$ following MBP or anti-CD3 Ab stimulation ($p < 0.01$). However, the increased $[Ca^{2+}]_i$ in the activated $CD4^+$ T cells from EAE rats was reduced by the ADWX-1 treatment at concentrations of 1 and 10 nM ($p < 0.05$, Fig. 3*A*). In contrast, ADWX-1 was less effective at inhibiting $[Ca^{2+}]_i$ in the activated $CD4^+$ T cells from the control rats (Fig. 3*A*). Furthermore, the ADWX-1 treatment dramatically reduced $[Ca^{2+}]_i$ in activated $CD4^+CCR7^-$ T cells, but not in $CD4^+CCR7^+$ T cells, from EAE (Fig. 3*B*) and control rats (Fig. 3*C*), likely because the IKCa1 channel (calcium-activated K^+ channel) modulates Ca^{2+} signaling in activated naive/T_{CM} cells in place of the Kv1.3 channel in T_{EM} cells (7, 25).

To further investigate the IL-2 activation pathway involved in the ADWX-1-induced blockade of the Kv1.3 channel, including the Ca^{2+} mediated NF-AT pathway and the PKCθ-triggered NF-κB pathway (Fig. 3*D*), we pretreated purified $CD4^+CCR7^-$ T cells from EAE rats with pathway-specific inhibitors followed by MBP stimulation in the presence or absence of ADWX-1. Cyclosporin A (CsA), a CaN inhibitor, was used to inhibit the NF-AT cascade to test the effect of ADWX-1 on the NF-κB pathway. Rottlerin, a PKCθ-specific inhibitor, was used to inhibit the NF-κB cascade to test the effect of ADWX-1 on the NF-AT pathway. The Mkb-triggered proliferation of inhibitor-treated cells was reduced in both cases (compared with mock-treated cells, in the absence of ADWX-1, the CsA-treated cells exhibited a reduction of ~40% and the PKCθ-treated cells exhibited a reduction of ~30%, Fig. 3*E*), suggesting that both pathways contribute to the antigen-induced cell activation and proliferation. In the CsA-treated NF-κB pathway, a decrease in proliferation was observed after the ADWX-1 treatment ($p < 0.001$, Fig. 3*E*), suggesting that ADWX-1 may be involved in regulating IL-2 activation and cell proliferation through the NF-κB pathway. In the rottlerin-treated NF-AT pathway, a decrease in proliferation was also observed after the ADWX-1 treatment ($p < 0.001$, Fig. 3*E*), suggesting that ADWX-1 signals through calcium modulation to trigger an inhibitory signaling cascade of NF-AT, which inhibits IL-2 activation and cell proliferation. The suppression of calcium in $CD4^+CCR7^-$ T cells by ADWX-1 is shown in Fig. 3*B*. When both inhibitors were introduced (CsA plus rottlerin), ADWX-1 exerted no apparent effect on proliferation ($p > 0.05$, Fig. 3*E*), suggesting that this peptide dose not affect any other IL-2 activation pathway.

Because the calcium signaling-mediated NF-AT pathway has been investigated using other Kv1.3 inhibitors (28), we specifically analyzed the effect of ADWX-1 on the Kv1.3-mediated Lck-PKCθ-NF-κB pathway in $CD4^+CCR7^-$ cells. Representative Western blots together with the densitometric quantifications of the phosphorylated activation of NF-κB are shown in Fig. 3, *F* and *G*. After antigen stimulation, the enhanced level of phosphorylated NF-κB (compared with the quiescent cells, $p < 0.05$) was suppressed by 1 nM ADWX-1, 10 nM ADWX-1 ($p < 0.05$), the PKCθ inhibitor rottlerin ($p < 0.05$), and the NF-κB inhibitor pyrrolidine dithiocarbamate ($p < 0.01$, Fig. 3*F*). Furthermore, we examined the activity of NF-κB following the activation of T cells from EAE and control rats. We observed that ADWX-1 preferentially reduces NF-κB activation in MBP-stimulated $CD4^+$ T cells from EAE rats ($p < 0.05$) but not in anti-CD3 Ab-stimulated cells from control rats ($p > 0.05$, Fig. 3*G*). These results suggest that the Kv1.3 channel is activated and recruited in the pathological state and that the Kv1.3 blocker ADWX-1 might specifically inhibit channel activity to modulate both the initial calcium signaling and the signaling events involved in NF-κB activation.

FIGURE 2. **Selective regulation of the $CD4^+CCR7^-$ T cell activation by ADWX-1.** *A,* representative FCM profile depicting CCR7 staining in CD4-gated PBMCs from each group; values in the *histogram* indicated the percentage of $CD4^+CCR7^-$ T cells. *B,* sorted $CD4^+CCR7^-$ and $CD4^+CCR7^+$ T cell populations in PBMCs from EAE rats were treated *in vitro* with 1 or 10 nM ADWX-1 or PBS (sham) 1 h before activation with MBP for 16 h. Resting control refers to quiescent cells in the base line. IL-2 levels in the supernatants were assessed by ELISA. *C,* sorted $CD4^+CCR7^-$ and $CD4^+CCR7^+$ T cell populations in PBMCs from control rats were treated as outlined in *B*; IL-2 secretion *in vitro* was assessed by ELISA. *D,* sorted human $CD4^+CCR7^-$ and $CD4^+CCR7^+$ T cells from three healthy donors were treated as outlined in *B*; IL-2 secretion *in vitro* was assessed by ELISA. ***, $p < 0.001$ *versus* activated (sham). The data represent the mean ± SD from three independent experiments performed in triplicate. *E, top panels,* $CD4^+CCR7^-$ T cells sorted from the PBMCs of EAE rats were previously CFSE-labeled and treated with (+) or without (−) 1 nM ADWX-1 and were stimulated with MBP for 96 h *in vitro*; the *numbers* in each gate are the percentage of proliferated cells assessed by CFSE staining. *Bottom panels,* total PBMCs from EAE rats were treated with (+) or without (−) 1 nM ADWX-1 before the stimulation with MBP for 96 h *in vitro*; the cells were gated on CD4, and *numbers* in each gate were the percentage of $CD4^+CCR7^-$ cells. The data are representative of two independent experiments.

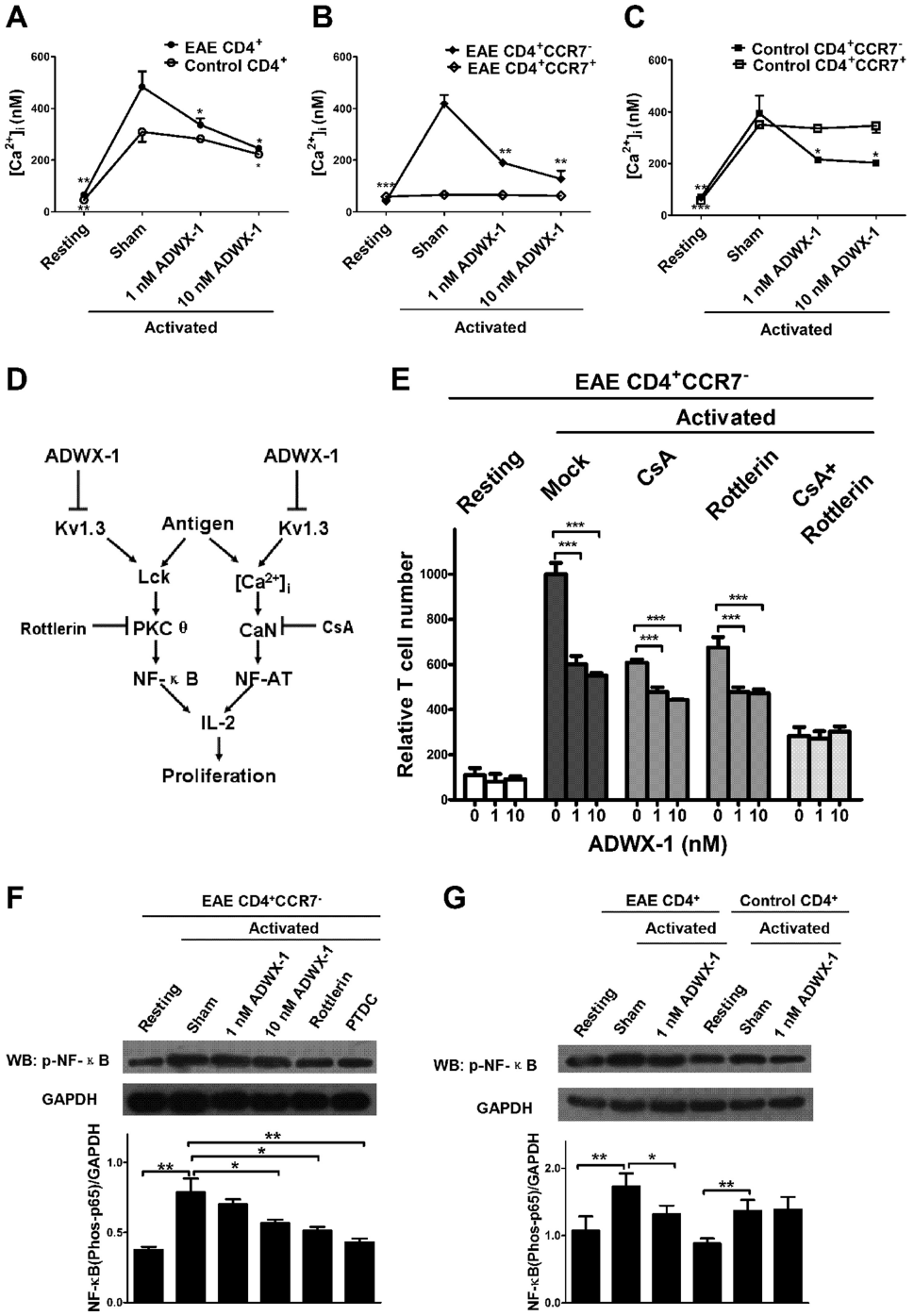

FIGURE 3. **Specific inhibitory effect of ADWX-1 on the $CD4^+CCR7^-$ subset IL-2 pathway.** *A,* calcium measurement. The sorted $CD4^+$ T cells from the PBMCs of EAE and control rats were loaded with Fura-2 AM and were preincubated with 1 or 10 nM ADWX-1 for 50 min. The cells were activated for 10 min with MBP or anti-CD3 Ab. $[Ca^{2+}]_i$ was calculated as the mean ± S.D. and is the representative of three independent experiments performed in duplicate. *B,* sorted $CD4^+CCR7^-$ and $CD4^+CCR7^+$ T cells from the PBMCs of EAE rats were treated as outlined in *A*, and $[Ca^{2+}]_i$ was calculated in the two populations. *C,* sorted $CD4^+CCR7^-$ and $CD4^+CCR7^+$ T cells from the PBMCs of control rats were treated as outlined in *A*, and $[Ca^{2+}]_i$ was calculated in the two populations. *, $p < 0.05$; **, $p < 0.01$; and ***, $p < 0.001$ *versus* activated (sham). *D,* schematic diagram of the ADWX-1-mediated anti-IL-2 activation mechanisms. ADWX-1 preferentially targets the Kv1.3 channels on $CD4^+CCR7^-$ T cells to prevent the Kv1.3-mediated downstream cascades for IL-2 activation, including the PKCθ pathway (*left*) and the calcium signaling pathway (*right*). *E,* $CD4^+CCR7^-$ T cells sorted from EAE rats were treated with CsA, rottlerin, or a combination of the two with the indicated concentrations of ADWX-1. After MBP stimulation, the normalized numbers of proliferated cells from Mock- (no inhibitor added), CsA-, rottlerin-, CsA + rottlerin-treated cells were analyzed. ***, $p < 0.001$ *versus* 0 nM ADWX-1. *F,* effects of 1 and 10 nM ADWX-1 on the PKCθ-NF-κB pathway in $CD4^+CCR7^-$ cells; the activities of NF-κB (phos-p65 Ser-536) stimulated by MBP were detected by Western blotting (*WB*), and the PKCθ-specific inhibitor rottlerin and the NF-κB inhibitor pyrrolidine dithiocarbamate were used as positive controls. The phosphorylation levels were quantified using Quantity One software, and the results are presented as a ratio to GAPDH. *G,* effects of 1 nM ADWX-1 on NF-κB activity in $CD4^+$ T cells from EAE (MBP-stimulated) and control (anti-CD3 Ab-stimulated) rats were detected by Western blotting. Proteins were analyzed as outlined in *F*. *, $p < 0.05$; **, $p < 0.01$ *versus* activated (sham). The data are the representative of three independent experiments performed in triplicate.

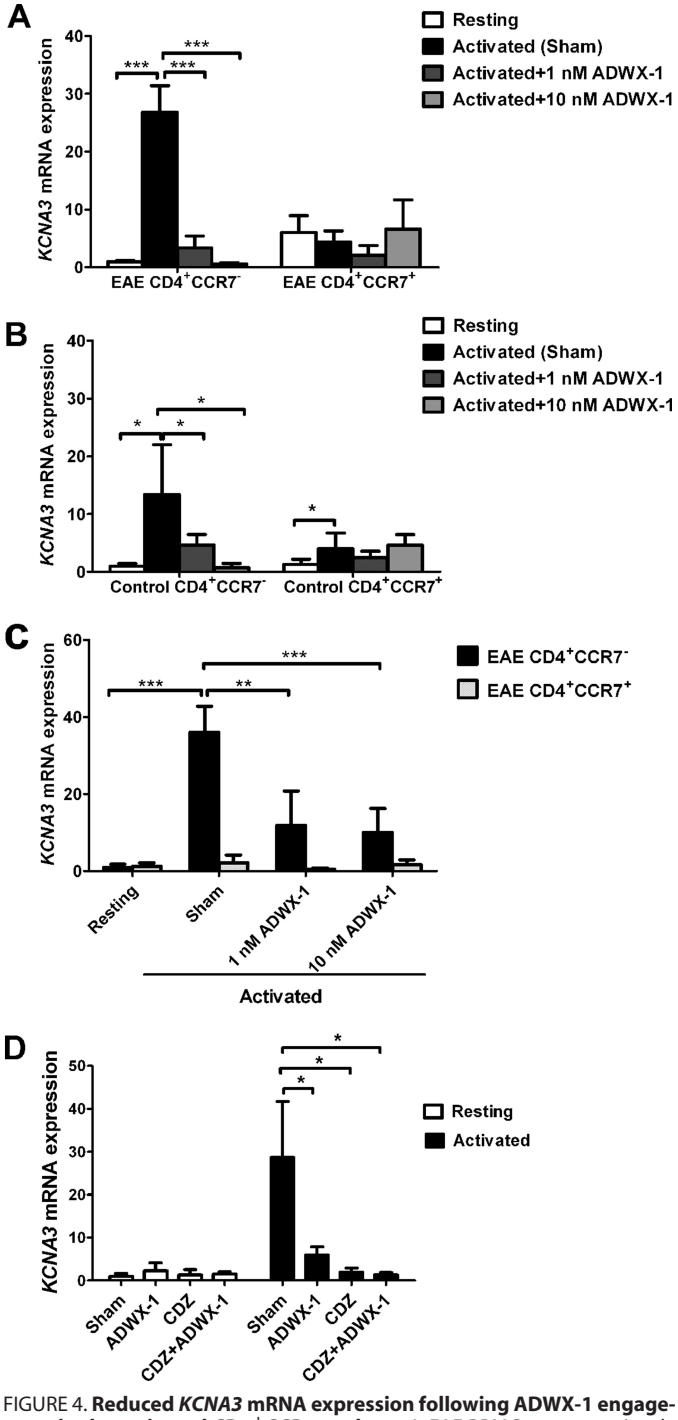

FIGURE 4. **Reduced *KCNA3* mRNA expression following ADWX-1 engagement in the activated $CD4^+CCR7^-$ subset.** *A,* EAE PBMCs were previously sorted for $CD4^+CCR7^-$ and $CD4^+CCR7^+$ cells, and the two populations were cultured with MBP for 48 h in the presence (1 or 10 nM) or absence (sham) of ADWX-1. The cells were harvested for the quantitative RT-PCR analysis of *KCNA3* (Kv1.3) mRNA levels. Resting $CD4^+CCR7^-$ T cell gene expression was used as the base line for gene expression, and all gene quantities were normalized to the expression of *GAPDH*. The relative mRNA expressions are representative of the mean ± S.D. from three independent experiments. *B,* pre-sorted $CD4^+CCR7^-$ and $CD4^+CCR7^+$ cells from PBMCs of control rats were treated as outlined in *A* with anti-CD3 Ab stimulation, and *KCNA3* mRNA expression was determined by quantitative RT-PCR analysis. *C,* EAE total PBMCs were cultured with MBP for 48 h in the presence (1 or 10 nM) or absence (sham) of ADWX-1, and the cells were harvested for sorting of $CD4^+CCR7^-$ (*black*) and $CD4^+CCR7^+$ (*white*) populations. The *KCNA3* mRNA expression in the two populations was determined by quantitative RT-PCR analysis. *, $p < 0.05$; **, $p < 0.01$, and ***, $p < 0.001$ *versus* activated (sham). *D,* $CD4^+CCR7^-$ T cells previously sorted from EAE rats were treated with 1 nM ADWX-1 or 10 μM CDZ or a combination of the two. After MBP activation, the amounts of *KCNA3* mRNA in each group were analyzed (*black*); the effects of the peptide and CDZ on the resting T cells were also determined (*white*). *, $p < 0.05$ *versus* sham group (no ADWX-1 or CDZ added).

ADWX-1 Preferentially Suppresses Kv1.3 Expression in Activated $CD4^+CCR7^-$ T Cell Subsets—Because the Kv1.3 channel is functionally responsible for the activation of $CD4^+CCR7^-$ T cells through the NF-AT- and NF-κB-mediated IL-2 pathways, we investigated whether the peptide with a high affinity for the Kv1.3 channel could selectively mediate the expression of Kv1.3 in $CD4^+CCR7^-$ T cells following activation. Our results show that the mRNA expression of the Kv1.3 gene (*KCNA3*) in pre-sorted $CD4^+CCR7^-$ T cells from EAE rats increased dramatically after antigen activation compared with resting cells ($p < 0.001$, Fig. 4*A*). However, the increased expression of *KCNA3* in the activated $CD4^+CCR7^-$ T cell subtype was significantly suppressed by ADWX-1 treatment when compared with sham-treated cells ($p < 0.001$, Fig. 4*A*). In contrast, no apparent up-regulation of *KCNA3* mRNA after antigen stimulation was observed in the pre-sorted $CD4^+CCR7^+$ T cells from the EAE rats, and ADWX-1 exhibited no significant effect on the activated T cells. Analogous selective effects of ADWX-1 were observed in cells from control rats stimulated with anti-CD3 Ab (Fig. 4*B*). Similarly, when the PBMCs from EAE rats were activated for 48 h before sorting into $CD4^+CCR7^-$ and $CD4^+CCR7^+$ populations for quantitative PCR analysis, the MBP stimuli significantly enhanced the *KCNA3* mRNA expression only in the $CD4^+CCR7^-$ T cells ($p < 0.001$). This increase was reversed significantly by 1 nM ADWX-1 ($p < 0.01$) and 10 nM ADWX-1 ($p < 0.001$, Fig. 4*C*).

Next we investigated the possible mechanisms underlying the modulation of the Kv1.3 expression by ADWX-1 in $CD4^+CCR7^-$ T cells. Using a bio-information forecast, a series of nuclear transcription factors targeting the cis-acting core motifs of the *KCNA3* 5′-flanking and 5′-noncoding region nucleotide sequence were identified, including the Ca^{2+}- and calmodulin-dependent nuclear factors nuclear factor of activated T-cells, Smad, cAMP-response element-binding protein, AP1, etc. Thus, we hypothesized that the high expression of the *KCNA3* gene following activation is associated with the initial calcium signaling mediated by Kv1.3 channel activity in the $CD4^+CCR7^-$ T cells. The calmodulin inhibitor calmidazolium (CDZ) was used to investigate the Ca^{2+} dependence of Kv1.3 expression. As shown in Fig. 4*D*, CDZ significantly decreased the high expression levels of *KCNA3* mRNA in the MBP-activated $CD4^+CCR7^-$ T cells ($p < 0.05$), suggesting that a calcium-dependent pathway might be involved in Kv1.3 expression. ADWX-1-treated (1 nM) cells did not exhibit lower *KCNA3* mRNA levels than the CDZ-treated cells (Fig. 4*D*), possibly because CDZ is a more potent inhibitor of Ca^{2+}/calmodulin than ADWX-1. When the CDZ and 1 nM ADWX-1 treatments were combined (CDZ + ADWX-1), the expression of *KCNA3* mRNA was slightly lower compared with CDZ treatment alone (Fig. 4*D*). In addition, ADWX-1 and CDZ had no significant effect on *KCNA3* mRNA expression in nonstimulated $CD4^+CCR7^-$ T cells (Fig. 4*D*). The results suggest that the selective modulation of calcium, shown in Fig. 3, *B* and *C*, is not

only responsible for NFAT activation but is also responsible for the selective regulation of Kv1.3 expression in $CD4^+CCR7^-$ T cells.

To confirm the selective effect of ADWX-1 on Kv1.3 expression at the protein level, we also measured the Kv1.3 expression by staining with a fluorescence-labeled antibody specific for Kv1.3 and gated on the $CD4^+CCR7^-$ and $CD4^+CCR7^+$ populations. The Kv1.3 protein expression was quantified by measuring the MFI of the Kv1.3 channels in the two gated populations ($CCR7^-$ and $CCR7^+$) of $CD4^+$ T cells (Fig. 5*A*). Within the overall PBMC system, the Kv1.3 MFI increased ~70% in the gated $CD4^+CCR7^-$ cell population following MBP activation ($p < 0.001$). ADWX-1 also selectively inhibited the Kv1.3 MFI at 1 nM ($p < 0.05$) and 10 nM ($p < 0.01$) in activated $CD4^+CCR7^-$ cells but not in $CD4^+CCR7^+$ cells (Fig. 5*A*). Furthermore, the Kv1.3 protein expression (MFI) increased ~64% following activation in the gated $CD4^+$ T cells from the PBMCs of EAE rats, whereas 1 and 10 nM ADWX-1 inhibited this increased expression by ~67 and 78%, respectively (Fig. 5*B*). Western blotting analysis was used to examine the membrane protein expression, and the results were consistent with the FCM data confirming the effect of ADWX-1 on Kv1.3 protein expression (Fig. 5*C*). The real time PCR, coupled with the FCM experiments, demonstrated that 1 and 10 nM doses of ADWX-1 decreased the high levels of Kv1.3 gene (*KCNA3*) expression following activation of the $CD4^+CCR7^-$ cells at both the mRNA and protein levels, which parallels the selective inhibitory effect of the peptide on the IL-2 pathway in $CD4^+CCR7^-$ cells.

To further examine the effect of ADWX-1 administration on the Kv1.3 expression in the gated $CD4^+$ T cells from the PBMCs of EAE rats *in vivo*, we measured the Kv1.3 MFI on freshly isolated T cells from ADWX-1-injected EAE rats. Compared with control rats, elevated Kv1.3 protein expression was observed in $CD4^+$ PBMCs from EAE rats (Fig. 5*D*). This observation is consistent with the high level of Kv1.3 expression in inflammatory infiltrates in the MS brain (8) because of the breakdown of the blood-brain barrier, and we speculate that the infiltrated cells may be auto-activated repeatedly in the peripheral circulation by myelin antigen injection. However, lower Kv1.3 expression levels were observed in ADWX-1-treated EAE rats when compared with vehicle-treated rats ($p < 0.01$, Fig. 5*D*). The effect of ADWX-1 on Kv1.3 expression *in vivo* suggests that ADWX-1 is responsible for the long term inhibition of activation of the $CCR7^-$ subtype, characterized by the enhanced Kv1.3 expression in the periphery.

ADWX-1 Regulates $CD4^+CCR7^-$ T Cell Restimulation—Considering the *in vivo* repeated activation of T cells in the EAE model, we tested the efficacy of ADWX-1 on T cell restimulation. Based on the channel expression tests above, we propose that the ability of $CD4^+CCR7^-$ T cells to reactivate might be impaired by ADWX-1 when the Kv1.3 expression is suppressed by ADWX-1 in the first stimulation. $CD4^+CCR7^-$ and $CD4^+CCR7^+$ T cells purified from EAE and control rats were pretreated with ADWX-1 during the first antigen activation. The cells were washed after 48 h and were allowed to rest for 3 days before rechallenging with antigen in the absence of ADWX-1. The restimulated $CD4^+CCR7^-$ subtype pretreated

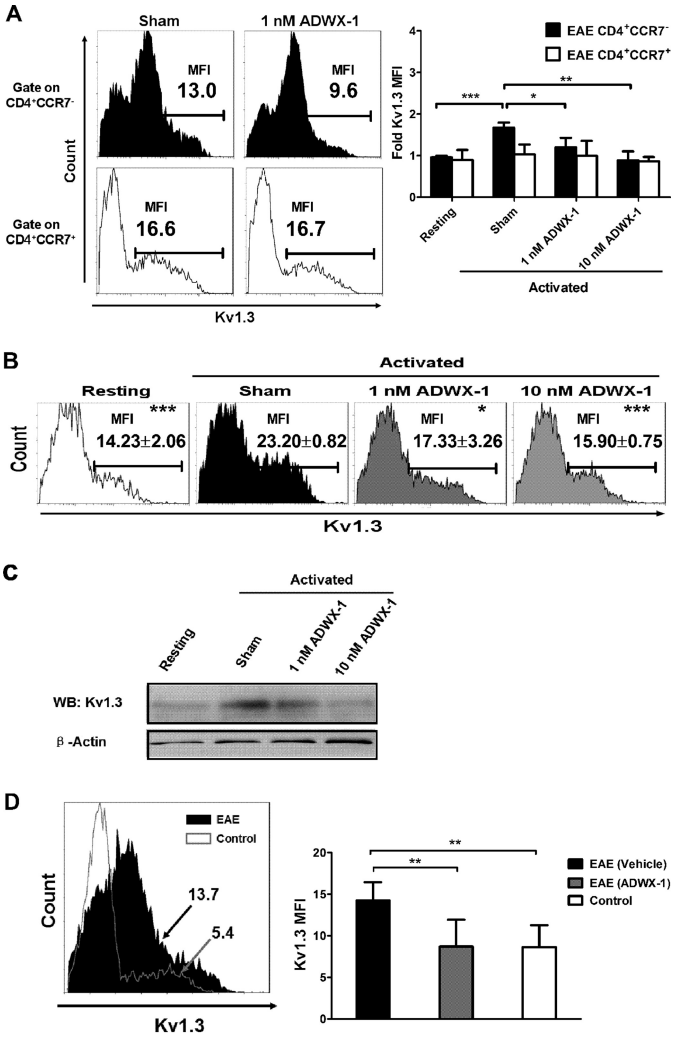

FIGURE 5. **Further modulation of Kv1. 3 protein expression by ADWX-1 in the activated $CD4^+CCR7^-$ subset.** *A,* EAE total PBMCs were treated as outlined in Fig. 4*C*; the cells were harvested for gating of $CD4^+CCR7^-$ (*black*) and $CD4^+CCR7^+$ (*white*) populations. The amounts of Kv1.3 MFI in the two populations were determined by FCM analysis. The representative Kv1.3 MFI in sham- or 1 nM ADWX-1-treated cells in the two populations are shown in the *histogram* (*left panels*). Statistical fold changes of the Kv1.3 MFI representing protein expression in the two populations from each group were determined using FCM (*right panel*). The Kv1.3 MFI in resting T cells was used as the base line for protein expression. *B,* Kv1.3 MFI measurement in the whole $CD4^+$ population gated from the cells in *A*; the numbers in the representative histograms are the mean ± S.D. of the Kv1.3 MFI values. *, $p < 0.05$; **, $p < 0.01$; and ***, $p < 0.001$ *versus* activated (sham). The data are representative of three independent experiments. *C,* membrane proteins were isolated from the EAE $CD4^+$ population (as outlined in *B*) for Western blot (*WB*) analysis of the Kv1.3 protein level to support the MFI data in *B*. *D,* Kv1.3 expression *in vivo*; the numbers in the histograms (*left panel*) are representative of the Kv1.3 MFI in the CD4-gated population of PBMCs from EAE (*black*) and control (*white*) rats; statistical Kv1.3 MFI in $CD4^+$ populations of PBMCs from each group ($n = 6$) were assessed (*right panel*). **, $p < 0.01$ *versus* EAE (vehicle).

with ADWX-1 in the first activation exhibited lower $[Ca^{2+}]_i$ compared with the non-ADWX-1-treated cells in both EAE ($p < 0.01$, Fig. 6*A*) and control rats ($p < 0.01$, Fig. 6*B*). The calcium regulation by ADWX-1 partly contributed to the peptide-mediated signaling of IL-2 activation. Consistently, the restimulation by antigens also resulted in significant IL-2 secretion ($p < 0.001$) in the $CD4^+CCR7^-$ T cells from both EAE (Fig. 6*C*) and control rats (Fig. 6*D*). However, the IL-2 levels in the supernatant of the sorted $CD4^+CCR7^-$ T cells from EAE (Fig.

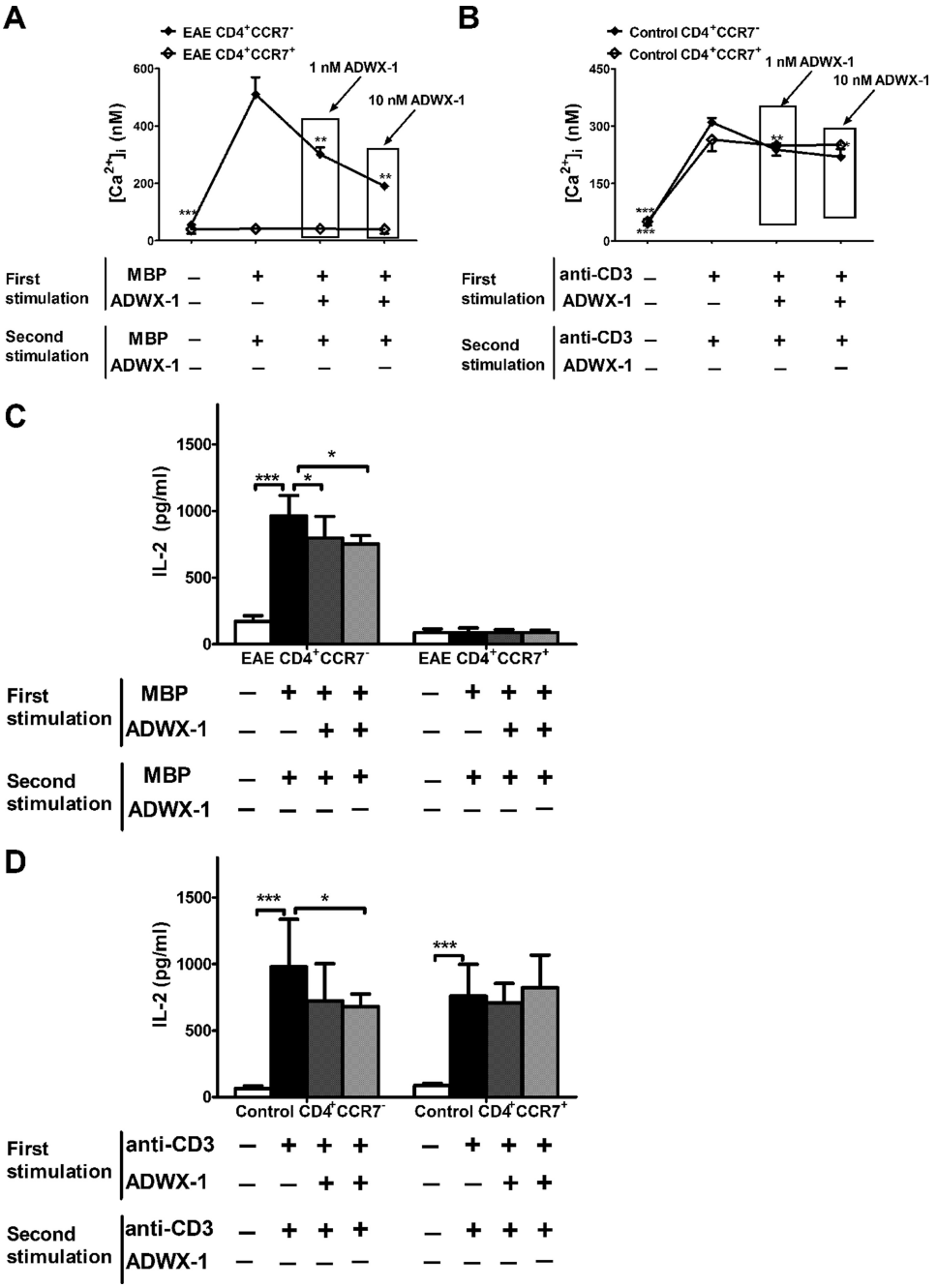

FIGURE 6. **Regulation of $CD4^+CCR7^-$ T restimulation by ADWX-1 pretreatment.** *A*, effect of ADWX-1 on $[Ca^{2+}]_i$ after restimulation. Sorted $CD4^+CCR7^-$ and $CD4^+CCR7^+$ T cells from the PBMCs of EAE rats were treated with antigen plus ADWX-1 for 48 h (ADWX-1 pretreated) and were reactivated by antigen alone for the calcium measurement. *B,* sorted cells from control rats were treated as outlined in *A* for the calcium measurement. *C* and *D,* after restimulation, the supernatants from the EAE group (*C*) and the control group (*D*) were collected for IL-2 measurement using ELISA. *, $p < 0.05$; **, $p < 0.01$, and ***, $p < 0.001$ *versus* reactivated group (first stimulation, antigen +, ADWX-1 −; Second stimulation, antigen +, ADWX-1 −). The data represent the mean ± S.D. from two independent experiments performed in triplicate.

6*C*) and control rats (Fig. 6*D*) also decreased ($p < 0.05$) when the cells were previously activated and treated with ADWX-1 before reactivation. Furthermore, no significant changes were observed in the supernatants from ADWX-1-pretreated $CD4^+CCR7^+$ T cells (Fig. 6, *C* and *D*). Therefore, the change in the Kv1.3 expression pattern induced by ADWX-1 produced a further and sustained inhibition of the $CD4^+CCR7^-$ phenotype where Kv1.3 activity was involved in the cell activation signal. The modulation of $CD4^+CCR7^-$ T cell reactivation *in vitro* by ADWX-1 also suggests that this peptide may physiologically inhibit the repeated activation of T_{EM} cells *in vivo*, thus preventing the high expression of Kv1.3 in the EAE model (Fig. 5*D*) with a parallel down-regulation of the number of $CD4^+CCR7^-$ T cells (Fig. 2*A*). The data indicate that the specific Kv1.3 blocker peptide ADWX-1 preferentially inhibits $CD4^+CCR7^-$ T cells activation, as evidenced by IL-2 production, through regulating both channel activity and channel expression.

ADWX-1 Suppresses Th17 Activation but Not Differentiation—Considering the effects of ADWX-1 on the activation and pro-

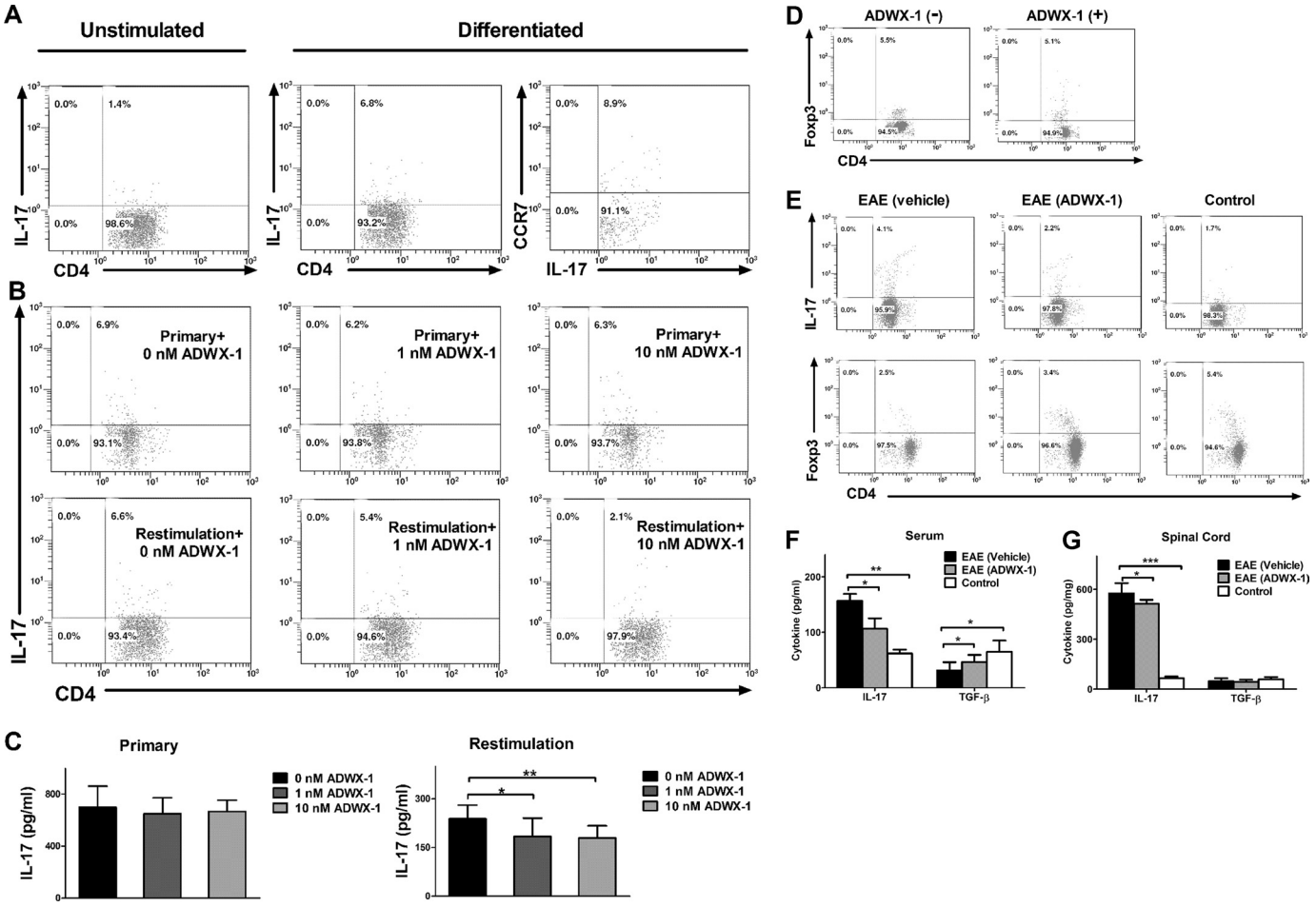

FIGURE 7. **Assessment of ADWX-1 in Th17 differentiation and EAE development.** *A,* dot plots showing the representative frequency of $CD4^+IL\text{-}17^+$ T cells when naive $CD4^+$ T cells were differentiated into Th17 using TGF-β and IL-6 plus anti-CD3/CD28 beads for 5 days; CD4 and IL-17 double-staining in *A* and *B* were gated on CD4. CCR7 phenotype in differentiated Th17 cells is shown in the *right panel*; CCR7 and IL-17 double-staining were gated on IL-17. *B, upper panels,* dot plots showing the frequency of $CD4^+IL\text{-}17^+$ T cells when naive $CD4^+$ T cells were incubated with 1 or 10 nM or without ADWX-1 during cytokine-induced differentiation. *Lower panels,* dot plots showing the frequency of $CD4^+IL\text{-}17^+$ T cells when the differentiated T cells were restimulated by anti-CD3 Ab and incubated with 1 to 10 nM or without ADWX-1 for 3 days. *C,* supernatants from *B* were analyzed using ELISA. IL-17 production from primary 5-day differentiated or overnight anti-CD3 Ab restimulated cultures were assessed in triplicate. *, $p < 0.05$; **, $p < 0.01$ *versus* 0 nM ADWX-1. The data are the representative of two independent experiments. *D,* dot plots showing the representative frequency of $CD4^+Foxp3^+$ T cells when $CD4^+$ T cells were activated by anti-CD3 Ab and incubated with 10 nM (+) or without ADWX-1 (−) for 3 days. CD4 and Foxp3 double-stained cells were gated on CD4. *E,* representative profiles exhibited the *in vivo* expression of $CD4^+IL\text{-}17^+$ and $CD4^+Foxp3^+$ T cells gated on CD4 using FCM. On day 15 post-immunization, the PBMC samples from each group ($n = 6$) were collected and were stained intracellularly. *F* and *G,* IL-17 and TGF-β levels in the serum (*F*) and the spinal cord (*G*) from each group ($n = 6$) were measured using ELISA. *, $p < 0.05$; **, $p < 0.01$, and ***, $p < 0.001$ *versus* EAE (vehicle).

liferation observed in $CD4^+$ T cells and because the polarization process requires antigen stimulation in addition to cytokine induction, we next investigated whether the modulation of $CD4^+$ T cell activation by ADWX-1 regulates $CD4^+IL\text{-}17^+$ T cell differentiation. In the absence of ADWX-1, ~7% of the rat naive $CD4^+$ T cells in culture was converted into $CD4^+IL\text{-}17^+$ cells by IL-6 and TGF-β induction (Fig. 7*A*), and the differentiated Th17 cells appeared mostly as the $CCR7^-$ phenotype (Fig. 7*A*). The cells differentiated in the presence of ADWX-1 exhibited no obvious differences in the numbers of $CD4^+IL\text{-}17^+$ cells compared with the cells differentiated in the absence of ADWX-1 (Fig. 7*B*). However, when the fully differentiated Th17 cells were restimulated with anti-CD3 Ab and were treated with ADWX-1, their expansion was suppressed compared with the untreated cells (Fig. 7*B*). The ELISA analysis of the primary culture supernatant, as well as the supernatants from effector Th17 cells restimulated with anti-CD3 Ab overnight, revealed a similar decrease in IL-17 production ($p < 0.05$ or $p < 0.01$) only in the restimulation culture in the presence of ADWX-1 (Fig. 7*C*). In addition, ADWX-1 did not exert a significant effect on $CD4^+Foxp3^+$ Treg cell proliferation *in vitro* (Fig. 7*D*). Our data suggest that ADWX-1 directly regulates the expansion of Th17 cells *in vitro* but not the differentiation of Th17 cells and that this efficacy is based on the cell selectivity of ADWX-1 on the $CD4^+CCR7^-$ T cells.

Furthermore, we used the EAE model to evaluate whether ADWX-1 targets mature Th17 *in vivo*. The administration of ADWX-1 prevented Th17 cell development in PBMCs (Fig. 7*E*) and slowed the progress of the disease, which resulted in a less severe decrease in $CD4^+Foxp3^+$ Treg cells compared with the model group (Fig. 7*E*). Consistently, IL-17 production in the serum of the EAE rats was reduced by ADWX-1 ($p < 0.05$) without further inhibition of TGF-β production (Fig. 7*F*). Furthermore, IL-17 production in the tissue (spinal cord) of EAE

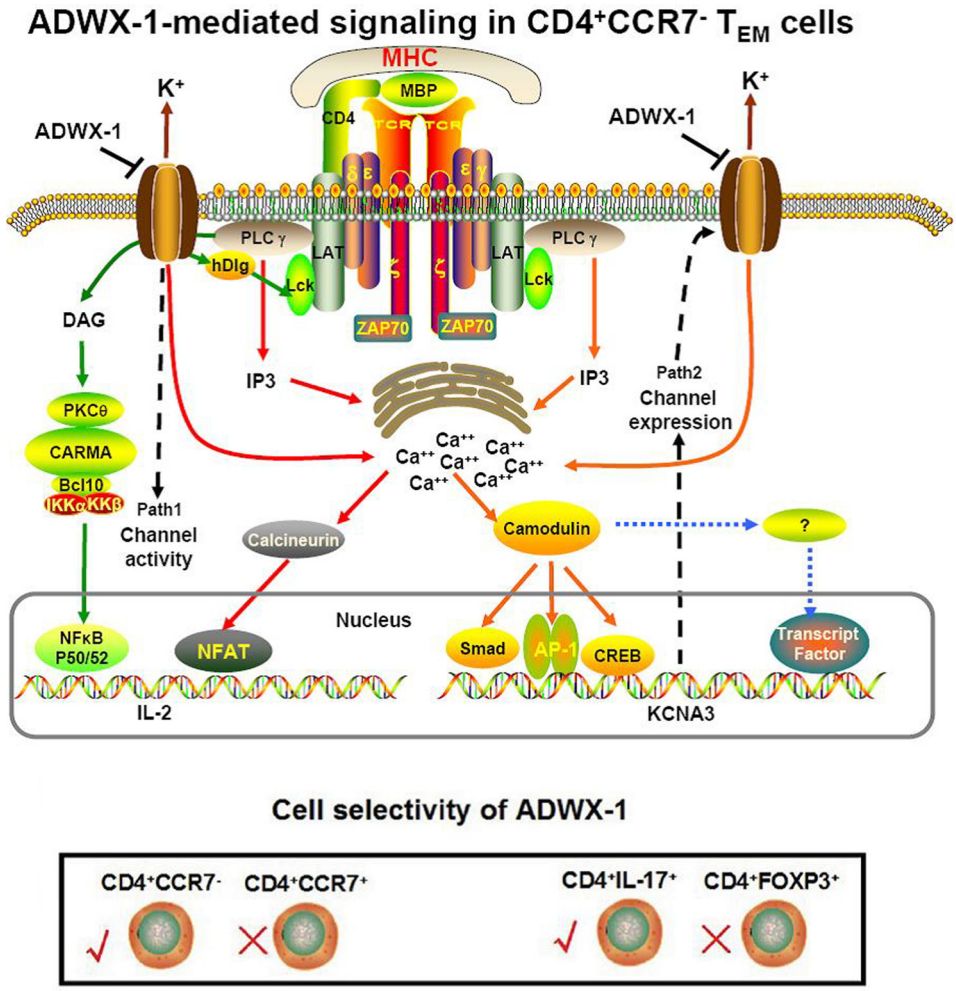

FIGURE 8. **Putative mechanisms of the effect of the Kv1. 3 blocker ADWX-1 on T_{EM} cells.** ADWX-1 preferentially inhibits $CD4^+CCR7^-$ T_{EM} subtype cells through two inhibitory pathways; one pathway mediates the transcriptional activation of IL-2 via NF-AT and NF-κB, and the other pathway regulates channel expression by affecting the binding of transcriptional factors to the Kv1.3 promoter via the upstream calcium signaling. This cell selectivity mechanism of ADWX-1 on $CD4^+CCR7^-/CCR7^+$ cells can be expanded to the activation of $CD4^+IL\text{-}17^+/CD4^+Foxp3^+$ cells.

rats decreased after ADWX-1 administration ($p < 0.05$), without any changes in TGF-β production in the CNS (Fig. 7*G*). These results demonstrate that ADWX-1 injection reduces Th17 generation *in vivo* and confers protection against EAE.

DISCUSSION

Using the rat EAE model, we have investigated the therapeutic effect of a novel Kv1.3 blocker peptide, ADWX-1, and the mechanisms underlying the treatment. Our data suggest that ADWX-1, designed from toxin as a specific blocker of the Kv1.3 channel, is a promising drug for the clinical therapy of MS. It has been reported that patients with multiple sclerosis exhibit high numbers of effector memory T cells characterized by a high levels of Kv1.3 expression, mainly because the numbers of Kv1.3 channels on activated $CD4^+CCR7^-CD45RA^-$ T_{EM} are significantly greater (~1,500) than on resting T_{EM} cells (~300) after repeated activation (7, 29). The difference in the number of channels following activation suggests that Kv1.3 is a promising drug target for T_{EM}-mediated autoimmune disease and the specific Kv1.3 blocker peptide ShK can suppress the proliferation of T_{EM} cells (5, 7, 30). Based on these data, we proposed that the novel Kv1.3 blocker peptide ADWX-1 exhibits cell selectivity between $CCR7^-$ T_{EM} and $CCR7^+$ naive/T_{CM} cells and that the preferential effect of ADWX-1 on the proliferation of T_{EM} cells might be associated with its regulation of the initial signals for cell activation.

In this study, our results suggest that ADWX-1 preferentially mediates the $CD4^+CCR7^-$ T_{EM} phenotype through two different inhibitory pathways (Fig. 8). One of these inhibitory pathways is the classic channel activity pattern in which IL-2 is transcriptionally activated by calcium-related nuclear factor NF-AT and the PKCθ-related nuclear factor NF-κB. The other pathway is the channel expression pattern in which the *KCNA3* gene expression is transcriptionally activated. Because Kv1.3 channels on $CD4^+CCR7^-$ T_{EM} cells modulate signals for the binding of nuclear factors to the *KCNA3* promoter, blocking the channel may functionally alter the transduction of the *KCNA3* promoter signaling and change the expression pattern of Kv1.3 on $CD4^+CCR7^-$ T_{EM} cells. In return, the expressed channels will influence cell reactivation. Therefore, ADWX-1 exhibits its inhibitory effect on the activation of $CD4^+$ $CCR7^-$ phenotype by regulating Kv1.3 from function to gene. Despite the report that hypoxia regulates the expression and activity of

Kv1.3 channels in T cell proliferation (31), the Kv1.3 blocker peptide ADWX-1 may directly mediate both the activity and expression of Kv1.3 channels in T_{EM} cell activation.

First, we determined that the Kv1.3 blocker ADWX-1 specifically inhibited the activation and subsequent proliferation of $CD4^+CCR7^-$ T_{EM} cells with a limited effect on $CD4^+CCR7^+$ naive/T_{CM} cells (Fig. 2, *B* and *C*). In the EAE model, $CD4^+CCR7^+$ T cells were less sensitive to MBP antigen stimulation, which is consistent with the observation that myelin-reactive T cells from MS patients are predominantly T_{EM} cells (7, 25). However, 1 nM ADWX-1 was more potent at inhibiting the activation of $CD4^+$ T cells from EAE rats than from the normal rats (data not shown). This observation is consistent with the effect of ADWX-1 on the total PBMCs *in vitro*, as shown in Fig. 1*F*, possibly because of the dominance of the $CD4^+CCR7^+$ naive/T_{CM} phenotype over the $CD4^+CCR7^-$ T_{EM} cell phenotype in normal rats (Fig. 2*A*). We also studied primary human T cells because they are physiologically similar to the human leukocyte microenvironment. The inhibitory effect of ADWX-1 on human T cells was similar to the reported effects of ShK on freshly isolated $CD4^+$ T cells, sorted T_{EM} cells, or chronic T_{EM} cells in humans (22).

Considering the question of how ADWX-1 modulates $CD4^+CCR7^-$ cell activation, we investigated the activation of the IL-2 (Fig. 3*D*). A non-calcium-dependent but Kv1.3-related IL-2 activation model that involves Lck and Kv1.3 may modulate TCR activation and downstream NF-κB events, and it is reported that Kv1.3, Kvβ2, SAP97, ZIP, and p56lck (Lck) co-cap with CD4 in human $CD4^+$ T_{EM} cells (25, 32). Because the physical association and functional correlation between active Lck and Kv1.3 channel activity have been examined (33), ADWX-1 targeting Kv1.3 might be associated with TCR signaling cascades via Lck in the early stages of T cell activation. A recent report claimed that the Disc large 1 (Dlg1)-tyrosine kinase Lck complex mediates protein kinase AI, which selectively regulates Kv1.3 channels in human T lymphocytes (34), proving the interaction of Lck, Kv1.3, and protein kinase. Because phosphorylation by Lck may be required to induce protein kinase C (PKC) activation (35, 36), and PKCθ as a member of PKC family selectively expresses on T lymphocyte, blocking the Kv1.3 channel may affect the function of Lck and the downstream signaling events for PKCθ activation (37). Furthermore, the downstream Carma1 complex transmits PKCθ signaling to IKKs, which ultimately phosphorylates the IκB in this cascade (38, 39).

It is remarkable that the specific Kv1.3 blocker peptide ADWX-1 regulates Kv1.3 channel expression on activated T_{EM} cells and that the expressed Kv1.3 channels are functionally important for the IL-2 activation of T_{EM} cells. We adopted two different cell culture sorting patterns for the assay of mRNA levels (Fig. 4, *A* and *C*). To rule out interference from other cells, we used the sorted cells ($CD4^+CCR7^-$/$CD4^+CCR7^+$) for ADWX-1 treatment *in vitro* to investigate the targeting function of ADWX-1 on the two cell subtypes. Meanwhile, the PBMCs from whole blood treated with ADWX-1 *in vitro* were used to evaluate the effect of the drug on the leukocyte microenvironment because the $CCR7^+$ and $CCR7^-$ subsets in $CD4^+$ T lymphocytes are physiologically mixed *in vivo*. Our results demonstrate that ADWX-1 selectively lowers the enhanced expression of Kv1.3 channels in $CD4^+CCR7^-$ T cells upon activation at both the mRNA and protein levels. In contrast, the enhancement of Kv1.3 expression was not apparent in the EAE $CD4^+CCR7^+$ T cells, and ADWX-1 had no effect on this subtype of T cells because the antigen-specific T cells were mainly $CD4^+CCR7^-$ T_{EM} $Kv1.3^{high}$ cells in MS/EAE (25). However, in control rats, although the $CD4^+CCR7^+$ cells responded to anti-CD3 Ab stimulation, the expression of the Kv1.3 channel increased only slightly without a substantial change in Kv1.3 expression on $CD4^+CCR7^+$ T cells after ADWX-1 treatment. It is likely that the activation of $CCR7^-$ cells depends on Kv1.3 channels but that $CCR7^+$ cell activation depends on IKCa1 channels, which exhibit functions that are equivalent to Kv1.3 (7, 25). Because the Kv1.3 channel is not mobilized in $CCR7^+$ cells, the level of Kv1.3 expression was not as high as in $CCR7^-$ cells and the Kv1.3 blocker ADWX-1 did not have a functional effect.

The effect of ADWX-1 on channel expression is similar to that reported for diclofenac, a nonsteroidal anti-inflammatory drug that inhibits Kv1.3 expression in activated T lymphocytes (40). However, diclofenac is not a specific Kv1.3 channel blocker, and the mechanism involved in its inhibition of Kv1.3 expression is unknown. In this study, we elucidated the tentative mechanism of the ADWX-1 peptide on channel expression based on the Kv1.3 promoter and Ca^{2+} signal transduction (Fig. 4*D*). Interestingly, the high expression of Kv1.3 in $CD4^+$ $CCR7^-$ T cells was dependent on calcium and calmodulin, and calcium signaling is in turn mediated by the Kv1.3 channel in this cell subtype (Fig. 3*B*); thus, there is a cross-talk between channel activity and channel expression in $CD4^+CCR7^-$ T cells. Furthermore, the lower Kv1.3 expression impairs the Kv1.3-dependent $CD4^+CCR7^-$ cell reactivation, which is Kv1.3-dependent; thus, pretreatment with ADWX-1 can also specifically lower IL-2 production in $CD4^+CCR7^-$ cells when they are restimulated (Fig. 6, *C* and *D*). However, the selective inhibition of channel expression differs from expression elimination by siRNA or other channel gene knockdown methods in that quiescent T cell channel expression remains unchanged after ADWX-1 treatment (Fig. 4*D*). Therefore, when compared with other identified immunological genes associated with the risk of developing MS (41), the changes in expression of *KCNA3* suggest that it is a gene that specifically regulates T_{EM} cells activation (41).

In addition to the classic Th1 type $CD4^+$ T cells, the latest studies show that Th17 and regulatory T cells (Treg) play vital roles in autoimmune diseases and inflammation. As a new lymphocyte subtype found in the EAE model, Th17 promotes inflammatory development, which is contrary to the anti-inflammatory role of Treg cells, and the receptors on the Th17 subsets contribute to their differentiation (42–44). To understand whether ADWX-1 affects the inflammatory Th17 cells, we shifted the focus of our research from cell proliferation to cell differentiation. The results showed that ADWX-1 did not suppress the Th17 cell polarization and IL-17 secretion *in vitro*, possibly because the cells were differentiated from naive $CD4^+$, which is a $CCR7^+$ phenotype, and that ADWX-1 was not effective in this type of cell. However, the peptide affected the restimulation of fully differentiated Th17 cells due to the

$CCR7^-$ phenotype in these polarized $CD4^+IL\text{-}17^+$ T cells. In contrast, there was no apparent change in $CCR7^+$-based Treg cells (45) after ADWX-1 treatment (Fig. 7*D*). Indeed, the $CCR7^+CD45RA^+$ naive T cells and the $CCR7^+CD45RA^-$ T_{CM} cells with the entry code of CCR7 were retained in the lymph node, whereas the $CCR7^-CD45RA^-$ T_{EM} cells without CCR7 infiltrated the inflamed tissue, resulting in effects such as cytokine secretion (5). The large proportion of $CCR7^-$ cells in the Th17 population accounts for the recruitment of Th17 to the lesion tissues in autoimmune diseases. The IL-17 levels were lowered in the tissue in particular following ADWX-1 treatment. Although Treg cells were down-regulated in the EAE model, ADWX-1 inhibited the exacerbation of the disease by suppressing Th17 cell development but not inhibiting the Treg cells further. These results demonstrate that ADWX-1 balances Th17 and Treg cells *in vivo* and ameliorates the MS/EAE disease. Similarly, studies of other peptides used for the treatment of MS report the involvement of Treg cells (46); however, the mechanisms for targeting Th17/Treg cells may differ for these peptides. The role of ADWX-1 in differentiation involves neither the replacement of cytokines, which trigger differentiation, nor synergy with cytokines to promote differentiation but rather the suppression of differentiated Th17 cells without affecting the Treg cells.

The selective effects of ADWX-1 on $CCR7^-$ T cell activation rather than on $CCR7^+$ T cells restore the balance of $CCR7^-$/$CCR7^+$ T cells, which might differ from the way Kv1.3 mediates the reversion of T effectors to central memory lymphocytes via cell cycle signaling (47). As a representative Kv1.3 blocker peptide, the mechanisms of ADWX-1 can be expanded to other Kv1.3-targeting toxin peptides or even to other chemical Kv1.3 blockers. The cell selectivity of ADWX-1 provides further support for the therapeutic potential of Kv1.3-specific channel blockers in T_{EM}-mediated autoimmune disease without side effects and broad immunosuppression (5, 48). At the same time, disease-associated autoreactive T cells in rheumatoid arthritis or type-1 diabetes mellitus patients mainly consist of $CD4^+CCR7^-CD45RA^-$ effector memory T cells (T_{EM} cells) with elevated Kv1.3 potassium channel expression, and ADWX-1 may ameliorate these diseases in rat models (25). Furthermore, it is reasonable to suggest ADWX-1 for broader immunotherapies in other effector memory T-related autoimmune diseases, such as psoriasis, chronic graft *versus* host disease, inflammatory bowel disease, and systemic lupus erythematosus.

In conclusion, the Kv1.3 blocker peptide ADWX-1 inhibited the excessive activation and proliferation of $CD4^+CCR7^-$ effector T cells by suppressing the channel activity-mediated IL-2 signaling and the expression of the Kv1.3 channel. Although MS is a multifocal demyelinating disease with multiple inducements, the multiple functions of ADWX-1, especially its dual inhibitory roles in both channel activity and channel expression in specific $CD4^+CCR7^-T_{EM}$ cells, make it a promising candidate drug for MS therapy.

Acknowledgment—We thank the Center for Medical Research of Wuhan University for providing the flow cytometry sample test and transmission electron microscopy image capture.

REFERENCES

1. Noseworthy, J. H., Lucchinetti, C., Rodriguez, M., and Weinshenker, B. G. (2000) Multiple sclerosis. *N. Engl. J. Med.* **343,** 938–952
2. Merrill, J. E. (2009) *In vitro* and *in vivo* pharmacological models to assess demyelination and remyelination. *Neuropsychopharmacology* **34,** 55–73
3. Nylander, A., and Hafler, D. A. (2012) Multiple sclerosis. *J. Clin. Invest.* **122,** 1180–1188
4. Goverman, J. (2009) Autoimmune T cell responses in the central nervous system. *Nat. Rev. Immunol.* **9,** 393–407
5. Beeton, C., Pennington, M. W., Wulff, H., Singh, S., Nugent, D., Crossley, G., Khaytin, I., Calabresi, P. A., Chen, C. Y., Gutman, G. A., and Chandy, K. G. (2005) Targeting effector memory T cells with a selective peptide inhibitor of Kv1.3 channels for therapy of autoimmune diseases. *Mol. Pharmacol.* **67,** 1369–1381
6. Rangaraju, S., Chi, V., Pennington, M. W., and Chandy, K. G. (2009) Kv1.3 potassium channels as a therapeutic target in multiple sclerosis. *Expert Opin. Ther. Targets* **13,** 909–924
7. Wulff, H., Calabresi, P. A., Allie, R., Yun, S., Pennington, M., Beeton, C., and Chandy, K. G. (2003) The voltage-gated Kv1.3 K^+ channel in effector memory T cells as new target for MS. *J. Clin. Invest.* **111,** 1703–1713
8. Rus, H., Pardo, C. A., Hu, L., Darrah, E., Cudrici, C., Niculescu, T., Niculescu, F., Mullen, K. M., Allie, R., Guo, L., Wulff, H., Beeton, C., Judge, S. I., Kerr, D. A., Knaus, H. G., Chandy, K. G., and Calabresi, P. A. (2005) The voltage-gated potassium channel Kv1.3 is highly expressed on inflammatory infiltrates in multiple sclerosis brain. *Proc. Natl. Acad. Sci. U.S.A.* **102,** 11094–11099
9. Beeton, C., Wulff, H., Singh, S., Botsko, S., Crossley, G., Gutman, G. A., Cahalan, M. D., Pennington, M., and Chandy, K. G. (2003) A novel fluorescent toxin to detect and investigate Kv1.3 channel up-regulation in chronically activated T lymphocytes. *J. Biol. Chem.* **278,** 9928–9937
10. Mouhat, S., Visan, V., Ananthakrishnan, S., Wulff, H., Andreotti, N., Grissmer, S., Darbon, H., De Waard, M., and Sabatier, J. M. (2005) K^+ channel types targeted by synthetic OSK1, a toxin from *Orthochirus scrobiculosus* scorpion venom. *Biochem. J.* **385,** 95–104
11. Garcia-Calvo, M., Leonard, R. J., Novick, J., Stevens, S. P., Schmalhofer, W., Kaczorowski, G. J., and Garcia, M. L. (1993) Purification, characterization, and biosynthesis of margatoxin, a component of *Centruroides margaritatus* venom that selectively inhibits voltage-dependent potassium channels. *J. Biol. Chem.* **268,** 18866–18874
12. Vennekamp, J., Wulff, H., Beeton, C., Calabresi, P. A., Grissmer, S., Hänsel, W., and Chandy, K. G. (2004) Kv1.3-blocking 5-phenylalkoxypsoralens. A new class of immunomodulators. *Mol. Pharmacol.* **65,** 1364–1374
13. Felix, J. P., Bugianesi, R. M., Schmalhofer, W. A., Borris, R., Goetz, M. A., Hensens, O. D., Bao, J. M., Kayser, F., Parsons, W. H., Rupprecht, K., Garcia, M. L., Kaczorowski, G. J., and Slaughter, R. S. (1999) Identification and biochemical characterization of a novel nortriterpene inhibitor of the human lymphocyte voltage-gated potassium channel, Kv1.3. *Biochemistry* **38,** 4922–4930
14. Chandy, K. G., Wulff, H., Beeton, C., Pennington, M., Gutman, G. A., and Cahalan, M. D. (2004) K^+ channels as targets for specific immunomodulation. *Trends Pharmacol. Sci.* **25,** 280–289
15. Takacs, Z., Toups, M., Kollewe, A., Johnson, E., Cuello, L. G., Driessens, G., Biancalana, M., Koide, A., Ponte, C. G., Perozo, E., Gajewski, T. F., Suarez-Kurtz, G., Koide, S., and Goldstein, S. A. (2009) A designer ligand specific for Kv1.3 channels from a scorpion neurotoxin-based library. *Proc. Natl. Acad. Sci. U.S.A.* **106,** 22211–22216
16. Han, S., Hu, Y., Zhang, R., Yi, H., Wei, J., Wu, Y., Cao, Z., Li, W., and He, X. (2011) ImKTx88, a novel selective Kv1.3 channel blocker derived from the scorpion *Isometrus maculates*. *Toxicon* **57,** 348–355
17. Chen, Z. Y., Hu, Y. T., Yang, W. S., He, Y. W., Feng, J., Wang, B., Zhao, R. M., Ding, J. P., Cao, Z. J., Li, W. X., and Wu, Y. L. (2012) Hg1, novel peptide inhibitor specific for Kv1.3 channels from first scorpion Kunitz-type potassium channel toxin family. *J. Biol. Chem.* **287,** 13813–13821
18. Beeton, C., Barbaria, J., Giraud, P., Devaux, J., Benoliel, A. M., Gola, M., Sabatier, J. M., Bernard, D., Crest, M., and Béraud, E. (2001) Selective blocking of voltage-gated K^+ channels improves experimental autoimmune encephalomyelitis and inhibits T cell activation. *J. Immunol.* **166,**

936–944
19. Beeton, C., Wulff, H., Barbaria, J., Clot-Faybesse, O., Pennington, M., Bernard, D., Cahalan, M. D., Chandy, K. G., and Béraud, E. (2001) Selective blockade of T lymphocyte K^+ channels ameliorates experimental autoimmune encephalomyelitis, a model for multiple sclerosis. *Proc. Natl. Acad. Sci. U.S.A.* **98,** 13942–13947
20. Han, S., Yi, H., Yin, S. J., Chen, Z. Y., Liu, H., Cao, Z. J., Wu, Y. L., and Li, W. X. (2008) Structural basis of a potent peptide inhibitor designed for Kv1.3 channel, a therapeutic target of autoimmune disease. *J. Biol. Chem.* **283,** 19058–19065
21. Yin, S. J., Jiang, L., Yi, H., Han, S., Yang, D. W., Liu, M. L., Liu, H., Cao, Z. J., Wu, Y. L., and Li, W. X. (2008) Different residues in channel turret determining the selectivity of ADWX-1 inhibitor peptide between Kv1.1 and Kv1.3 channels. *J. Proteome Res.* **7,** 4890–4897
22. Hu, L., Pennington, M., Jiang, Q., Whartenby, K. A., and Calabresi, P. A. (2007) Characterization of the functional properties of the voltage-gated potassium channel Kv1.3 in human $CD4^+$ T lymphocytes. *J. Immunol.* **179,** 4563–4570
23. Merrill, J. E., Hanak, S., Pu, S. F., Liang, J., Dang, C., Iglesias-Bregna, D., Harvey, B., Zhu, B., and McMonagle-Strucko, K. (2009) Teriflunomide reduces behavioral, electrophysiological, and histopathological deficits in the Dark Agouti rat model of experimental autoimmune encephalomyelitis. *J. Neurol.* **256,** 89–103
24. Paintlia, A. S., Paintlia, M. K., Singh, I., and Singh, A. K. (2008) Combined medication of lovastatin with rolipram suppresses severity of experimental autoimmune encephalomyelitis. *Exp. Neurol.* **214,** 168–180
25. Beeton, C., Wulff, H., Standifer, N. E., Azam, P., Mullen, K. M., Pennington, M. W., Kolski-Andreaco, A., Wei, E., Grino, A., Counts, D. R., Wang, P. H., LeeHealey, C. J., S Andrews, B., Sankaranarayanan, A., Homerick, D., Roeck, W. W., Tehranzadeh, J., Stanhope, K. L., Zimin, P., Havel, P. J., Griffey, S., Knaus, H. G., Nepom, G. T., Gutman, G. A., Calabresi, P. A., and Chandy, K. G. (2006) Kv1.3 channels are a therapeutic target for T cell-mediated autoimmune diseases. *Proc. Natl. Acad. Sci. U.S.A.* **103,** 17414–17419
26. Feske, S., Giltnane, J., Dolmetsch, R., Staudt, L. M., and Rao, A. (2001) Gene regulation mediated by calcium signals in T lymphocytes. *Nat. Immunol.* **2,** 316–324
27. Feske, S. (2007) Calcium signaling in lymphocyte activation and disease. *Nat. Rev. Immunol.* **7,** 690–702
28. Ren, Y. R., Pan, F., Parvez, S., Fleig, A., Chong, C. R., Xu, J., Dang, Y., Zhang, J., Jiang, H., Penner, R., and Liu, J. O. (2008) Clofazimine inhibits human Kv1.3 potassium channel by perturbing calcium oscillation in T lymphocytes. *PloS one* **3,** e4009
29. Beeton, C., and Chandy, K. G. (2005) Potassium channels, memory T cells, and multiple sclerosis. *Neuroscientist* **11,** 550–562
30. Wulff, H., Castle, N. A., and Pardo, L. A. (2009) Voltage-gated potassium channels as therapeutic targets. *Nat. Rev. Drug Discov.* **8,** 982–1001
31. Conforti, L., Petrovic, M., Mohammad, D., Lee, S., Ma, Q., Barone, S., and Filipovich, A. H. (2003) Hypoxia regulates expression and activity of Kv1.3 channels in T lymphocytes. A possible role in T cell proliferation. *J. Immunol.* **170,** 695–702
32. Cahalan, M. D., and Chandy, K. G. (2009) The functional network of ion channels in T lymphocytes. *Immunol. Rev.* **231,** 59–87
33. Szigligeti, P., Neumeier, L., Duke, E., Chougnet, C., Takimoto, K., Lee, S. M., Filipovich, A. H., and Conforti, L. (2006) Signaling during hypoxia in human T lymphocytes. Critical role of the Src protein tyrosine kinase p56Lck in the O2 sensitivity of Kv1.3 channels. *J. Physiol.* **573,** 357–370
34. Kuras, Z., Kucher, V., Gordon, S. M., Neumeier, L., Chimote, A. A., Filipovich, A. H., and Conforti, L. (2012) Modulation of K(V)1.3 channels by protein kinase AI in T lymphocytes is mediated by the disc large L-tyrosine kinase Lck complex. *Am. J. Physiol. Cell Physiol.* **302,** 1504
35. Hayashi, K., and Altman, A. (2007) Protein kinase Cθ (PKCθ). A key player in T cell life and death. *Pharmacol. Res.* **55,** 537–544
36. Melowic, H. R., Stahelin, R. V., Blatner, N. R., Tian, W., Hayashi, K., Altman, A., and Cho, W. (2007) Mechanism of diacylglycerol-induced membrane targeting and activation of protein kinase Cθ. *J. Biol. Chem.* **282,** 21467–21476
37. Smith-Garvin, J. E., Koretzky, G. A., and Jordan, M. S. (2009) T cell activation. *Annu. Rev. Immunol.* **27,** 591–619
38. Matsumoto, R., Wang, D., Blonska, M., Li, H., Kobayashi, M., Pappu, B., Chen, Y., Wang, D., and Lin, X. (2005) Phosphorylation of CARMA1 plays a critical role in T cell receptor-mediated NF-κB activation. *Immunity* **23,** 575–585
39. Rueda, D., and Thome, M. (2005) Phosphorylation of CARMA1. The link(er) to NF-κB activation. *Immunity* **23,** 551–553
40. Villalonga, N., David, M., Bielańka, J., González, T., Parra, D., Soler, C., Comes, N., Valenzuela, C., and Felipe, A. (2010) Immunomodulatory effects of diclofenac in leukocytes through the targeting of Kv1.3 voltage-dependent potassium channels. *Biochem. Pharmacol.* **80,** 858–866
41. Fugger, L., Friese, M. A., and Bell, J. I. (2009) From genes to function. The next challenge to understanding multiple sclerosis. *Nat. Rev. Immunol.* **9,** 408–417
42. Quintana, F. J., Basso, A. S., Iglesias, A. H., Korn, T., Farez, M. F., Bettelli, E., Caccamo, M., Oukka, M., and Weiner, H. L. (2008) Control of T(reg) and T(H)17 cell differentiation by the aryl hydrocarbon receptor. *Nature* **453,** 65–71
43. Gulen, M. F., Kang, Z., Bulek, K., Youzhong, W., Kim, T. W., Chen, Y., Altuntas, C. Z., Sass Bak-Jensen, K., McGeachy, M. J., Do, J. S., Xiao, H., Delgoffe, G. M., Min, B., Powell, J. D., Tuohy, V. K., Cua, D. J., and Li, X. (2010) The receptor SIGIRR suppresses Th17 cell proliferation via inhibition of the interleukin-1 receptor pathway and mTOR kinase activation. *Immunity* **32,** 54–66
44. Farez, M. F., Quintana, F. J., Gandhi, R., Izquierdo, G., Lucas, M., and Weiner, H. L. (2009) Toll-like receptor 2 and poly(ADP-ribose) polymerase 1 promote central nervous system neuroinflammation in progressive EAE. *Nat. Immunol.* **10,** 958–964
45. Schneider, M. A., Meingassner, J. G., Lipp, M., Moore, H. D., and Rot, A. (2007) CCR7 is required for the *in vivo* function of $CD4^+$ $CD25^+$ regulatory T cells. *J. Exp. Med.* **204,** 735–745
46. Shapira, E., Brodsky, B., Proscura, E., Nyska, A., Erlanger-Rosengarten, A., and Wormser, U. (2010) Amelioration of experimental autoimmune encephalitis by novel peptides. Involvement of T regulatory cells. *J. Autoimmun* **35,** 98–106
47. Hu, L., Gocke, A. R., Knapp, E., Rosenzweig, J. M., Grishkan, I. V., Baxi, E. G., Zhang, H., Margolick, J. B., Whartenby, K. A., and Calabresi, P. A. (2012) Functional blockade of the voltage-gated potassium channel Kv1.3 mediates reversion of T effector to central memory lymphocytes through SMAD3/p21cip1 signaling. *J. Biol. Chem.* **287,** 1261–1268
48. Matheu, M. P., Beeton, C., Garcia, A., Chi, V., Rangaraju, S., Safrina, O., Monaghan, K., Uemura, M. I., Li, D., Pal, S., de la Maza, L. M., Monuki, E., Flügel, A., Pennington, M. W., Parker, I., Chandy, K. G., and Cahalan, M. D. (2008) Imaging of effector memory T cells during a delayed-type hypersensitivity reaction and suppression by Kv1.3 channel block. *Immunity* **29,** 602–614